Full-switching FSF-type superconducting spin-triplet magnetic random access memory element

D. Lenk,[1] R. Morari,[1,2] V. I. Zdravkov,[1,2] A. Ullrich,[1] Yu. Khaydukov,[3] G. Obermeier,[1] C. Müller,[1] A. S. Sidorenko,[2] H.-A. Krug von Nidda,[1] S. Horn,[1] L. R. Tagirov,[1,4,5] and R. Tidecks[1]

[1]*Universität Augsburg, Universitätsstraße 1, D-86159 Augsburg, Germany*

[2]*D. Ghitsu Institute of Electronic Engineering and Nanotechnologies ASM, Academiei Str. 3/3, MD2028 Kishinev, Moldova*

[3]*Max-Planck-Institut für Festkörperforschung, Heisenbergstraße 1, D-70569 Stuttgart, Germany*

[4]*Zavoisky Physical-Technical Institute, Kazan Scientific Center of RAS, Sibirsky tract 10/7, 420029 Kazan, Russian Federation*

[5]*Institute of Physics, Kazan Federal University, Kremlevskaya Str. 18, 420008 Kazan, Russian Federation*

(Received 13 October 2016; revised manuscript received 20 July 2017; published 27 November 2017)

In the present work a superconducting Co/CoO_x/$Cu_{41}Ni_{59}$/Nb/$Cu_{41}Ni_{59}$ nanoscale thin film heterostructure is investigated, which exhibits a superconducting transition temperature, T_c, depending on the history of magnetic field applied parallel to the film plane. In more detail, around zero applied field, T_c is lower when the field is changed from negative to positive polarity (with respect to the cooling field), compared to the opposite case. We interpret this finding as the result of the generation of the odd-in-frequency triplet component of superconductivity arising at noncollinear orientation of the magnetizations in the $Cu_{41}Ni_{59}$ layer adjacent to the CoO_x layer. This interpretation is supported by superconducting quantum interference device magnetometry, which revealed a correlation between details of the magnetic structure and the observed superconducting spin-valve effects. Readout of information is possible at zero applied field and, thus, no permanent field is required to stabilize both states. Consequently, this system represents a superconducting magnetic random access memory element for superconducting electronics. By applying increased transport currents, the system can be driven to the full switching mode between the completely superconducting and the normal state.

DOI: 10.1103/PhysRevB.96.184521

I. INTRODUCTION

The possible existence of a superconducting state in a spin-split electron system (i.e., in the presence of an exchange field) was theoretically predicted already a long time ago by Fulde-Ferrell [1] and Larkin-Ovchinnikov [2] (FFLO). However, experimental evidence is scarce [3], because the spin-alignment tendency of ferromagnetism is in direct conflict with spin-singlet superconductivity generated by electron pairs (Cooper pairs) of opposite spin [4].

More recently a quasi-one-dimensional FFLO-like state was theoretically predicted [5–7] in thin-film heterostructures of superconductors (S) and ferromagnets (F). Similar to the exponential decay of the pairing wave function (PWF) in the normal conductor (N) of a proximity coupled S/N bilayer, the amplitude of the PWF in the F material shows an exponential decay (however with a different decay length). Moreover, the PWF oscillates as a function of space normal to the film plane. The reflection of the PWF (e.g., at the outer boundary of the F layer of a S/F bilayer) can lead to interference effects [5,8–10] and, thus, to an oscillating superconducting transition temperature, T_c, as a function of the thickness of the ferromagnetic layer, d_F. For an optimized set of parameters [5,8–10], superconductivity can even vanish at certain d_F and recover at even higher d_F.

A possible application of the quasi-one-dimensional FFLO-like state is based on superconductors combined with at least two ferromagnetic layers. In such systems T_c not only depends on the structural properties of the sample, but also on the relative magnetization directions of the constituent ferromagnetic layers (similar to the giant magnetoresistance (GMR) effect [11,12], exploited in F/N/F spin-valves [13], which is, however, based on different physics). For a working temperature between the two superconducting transition temperatures of different magnetic states, it is, thus, possible to switch the structure between the superconducting and the normal conducting state by switching the magnetic state. Thus, these systems represent superconducting spin-valves (SSVs). In the literature, both the direct or standard SSV effect (i.e., T_c is higher for antiparallel than for parallel alignment of the magnetizations) and the inverse SSV effect (opposite case) are predicted theoretically [14–21] and found experimentally in F/S/F-type [22–40] and S/F/F-type [41–45] structures. Moreover, a triplet SSV effect, i.e., an absolute minimum of T_c at noncollinear alignment of the magnetizations is predicted theoretically for S/F/F-type SSVs in the dirty [19,21] and clean limit [46], and F/S/F-type SSVs only in the clean limit [20]. This effect is based on the generation of a superconducting long-range odd-in-frequency s-wave triplet pairing component with spin-projection one. This triplet component is coupled to the zero spin-projection triplet and the singlet component and, thus, only indirectly enters the self-consistency equation, which determines the superconducting gap and includes the singlet component [18,19,21] only. The generation of triplet charge carriers with spin-projection one exhausts the singlet component and, thus, reduces the superconducting gap and, consequently, T_c.

While the triplet SSV effect has been introduced as absolute minimum of T_c at noncollinear alignment of the magnetizations of two distinct ferromagnetic layers [19], the term has also been used in the broader sense of a T_c reduction, arising from the influence of arbitrary noncollinear magnetic spins on the superconductor. We explicitly note that we will adopt this broader sense in the following. Recently, experimental evidence of the triplet SSV effect in S/F/F-type SSVs [47–55], as well as F/S/F-type SSVs [52,56,57] has been obtained.

In the present paper, we investigate the triplet SSV effect in a F/S/F-type SSV, consisting of a $Cu_{41}Ni_{59}$/Nb/$Cu_{41}Ni_{59}$ core on antiferromagnetic CoO_x with a Co sublayer to modify the

magnetic properties of the lower $Cu_{41}Ni_{59}$-layer by exchange biasing [58] the Co and bottom $Cu_{41}Ni_{59}$ layer and interlayer coupling between both layers [58]. While first results on such samples have been presented in our previous work [57], the present study is intended to investigate the origin of the triplet SSV effect in this system in more detail and find optimized working parameters (from an application point of view). We develop a set of working parameters to manifest full switching, i.e., a change of the system from a completely superconducting to the normal conducting state by a change of the magnetic history.

According to Robinson [59], triplet SSVs can serve similar purposes as normal conducting GMR devices, e.g., as magnetic random access memory (MRAM) elements [60], however, with the potential for much higher efficiency. Since in the present system, readout of information is possible at zero applied field and, thus, no permanent field is required to stabilize both states, the system investigated represents a superconducting MRAM element for spintronics [61].

Also the standard or inverse SSV effect can provide the basis for an MRAM element, if the system has suitable magnetic hysteresis properties, i.e., the superconducting transition temperature at the two resulting magnetic configurations at zero field have to be different (see, e.g., Refs. [22,25,26,37,38,49,50,52,62]).

Recently, Li *et al.* [63] developed a MRAM element, switching between a fully normal conducting and a fully superconducting state, using a FI/S/FI SSV, where FI denotes a ferromagnetic insulator. However, as discussed in detail in Appendix A of the present paper, the underlying physical mechanism is different from the proximity based effects arising using conducting ferromagnets.

II. SAMPLE PREPARATION AND CHARACTERIZATION

The sample in the present work has been selected from a $Co/CoO_x/Cu_{41}Ni_{59}/Nb/Cu_{41}Ni_{59}$ sample series deposited on a Si substrate by magnetron sputtering (for details of the preparation see our previous work [57]). While all other layers are intended to be of constant thickness, the thicknesses of both $Cu_{41}Ni_{59}$ layers change across the sample series. Since the change of these thicknesses between neighboring samples is small compared to the characteristic scales of the effect to be investigated, the thickness in each individual sample can be regarded as constant with sufficient accuracy.

The intended structure of the sample series is confirmed by transmission electron microscopy (TEM) and Rutherford backscattering spectroscopy (RBS). Figure 1 shows examples of TEM images (for a sample with thicker $Cu_{41}Ni_{59}$ layers than in the present study). The structure of the sample is indicated by assigning the materials of the layers. All layers show highly crystalline structure, the interfaces between the individual layers are smooth and clean (which is the case for all investigated samples). While the top panel shows the overall structure, the bottom panel shows an image of the Co sublayer, the CoO_x, and the adjacent regions at higher magnification. The lattice spacing of the Si substrate has been analyzed in detail to calibrate the scale. The layer thicknesses, obtained by TEM, and linear interpolations between these values have been used as initial values to fit the RBS spectra.

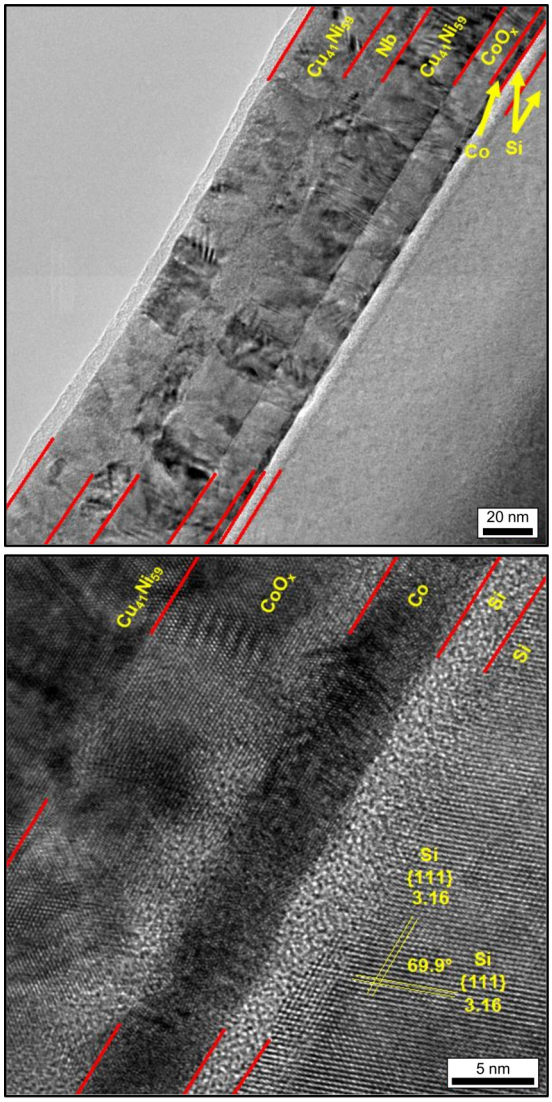

FIG. 1. Cross-sectional TEM images of a sample of the same series as the investigated one, however, with thicker $Cu_{41}Ni_{59}$ layers. Top: Overview of the layered structure. Bottom: High-resolution image of the Co sublayer, the CoO_x, and the adjacent regions. The Si substrate was covered by a Si buffer layer, before deposition of the heterostructure. The structure was finished by sealing it against oxidation by a Si cap. The lattice spacing of the Si substrate (right bottom corner) has been analyzed in detail to calibrate the scale.

This is necessary because, due to the similar atomic mass of Cu, Ni, and Co, and the low sensitivity for O, the spectra are not unambiguously fittable without external information. The layer thicknesses for the investigated sample are obtained by averaging the RBS results for both adjacent samples (the investigated sample is not subjected to RBS to avoid radiation damage). Figure 2 shows the spectrum of the thinner next sample together with the fit. While the left panel shows the full spectrum, the right panel shows the energy range of the peaks associated with the functional layers in more detail. There is good agreement between the fit and the experimental data. The layer thicknesses obtained for the Co, the CoO_x, the bottom $Cu_{41}Ni_{59}$, the Nb, and the top $Cu_{41}Ni_{59}$ layer of

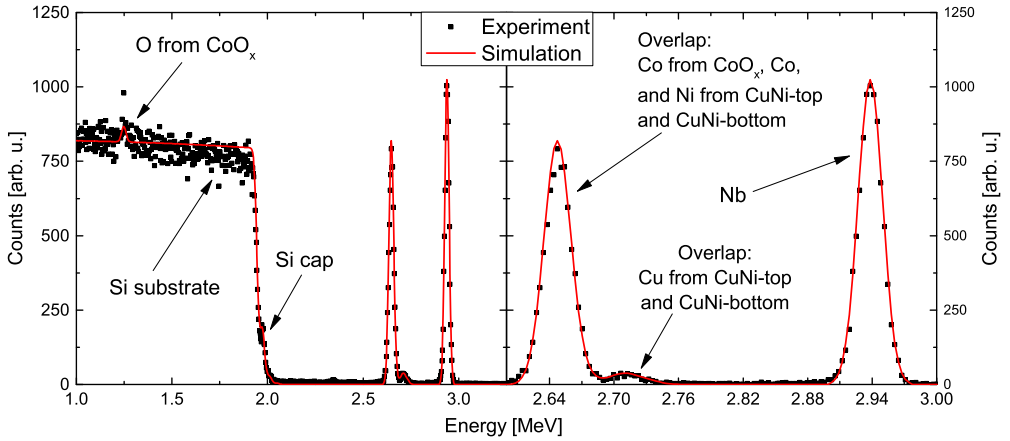

FIG. 2. RBS spectrum of the sample adjacent to the sample investigated in the present paper (with slightly thinner $Cu_{41}Ni_{59}$ layers). Left: Entire spectrum. Right: Enlarged view of the energy range of the peaks associated to the functional layers.

the investigated sample are 4.6, 16.0, 2.2, 11.4, and 2.5 nm, respectively.

III. RESULTS AND DISCUSSION

A. Transport measurements

The triplet SSV effect was investigated by collecting resistance-temperature, R(T), measurements to determine the superconducting transition temperature, T_c, at different magnetic detection fields, H_D, applied parallel to the film plane.

The measurements were performed in an Oxford Instruments Heliox sorption pumped ^{3}He insert. The resistance was measured using a four-probe method. Unless otherwise stated explicitly, the resistive measurements were performed using a lock-in technique with a current of 50 μA at a frequency of 18.792 Hz.

The sample was cooled down to liquid helium temperature in a field of +70 kOe ($\widehat{=}$ 7.0 T in SI units [64]), applied in the film plane. Subsequently, the magnetic state was trained [65] by alternating application of −70 kOe and +70 kOe several times, to ensure stability of the magnetic state. The magnetic field dependence of the transition temperature, $T_c(H_D)$, was obtained by measuring R(T) transition curves for decreasing and increasing temperature at various fixed H_D, from 70 kOe to −70 kOe and vice versa, (see Sec. III D for a characteristic transition curve, the values of T_c have been evaluated as the temperature related to half of the normal state resistance).

A broad hysteresis of T_c as a function of the detection field [similar to the one labeled $H_S = 4.0$ kOe in Fig. 3(a)] is observed, i.e., T_c depends not only on H_D, but on the magnetic history. We interpret this finding to be based on the generation of the long-range odd-in-frequency triplet pairing component, arising when a noncollinear relative orientation of the magnetic moments in the bottom $Cu_{41}Ni_{59}$ layer is obtained, yielding a reduction of T_c around zero field for increasing H_D (for a detailed discussion, see Sec. III B). Since the range of reduction of T_c is broad, it is hard to assign a characteristic field, correlated to the generation of the triplet component.

To find such a characteristic field, we performed minor loop measurements, i.e., the maximum absolute value of field, H_S, applied before reversal of the direction of H_D change (in the following denoted as reversal field) is stepwise reduced below 70 kOe. Consequently, H_D is only varied between H_S and $-H_S$ and vice versa, with $H_S < 70$ kOe. However, no

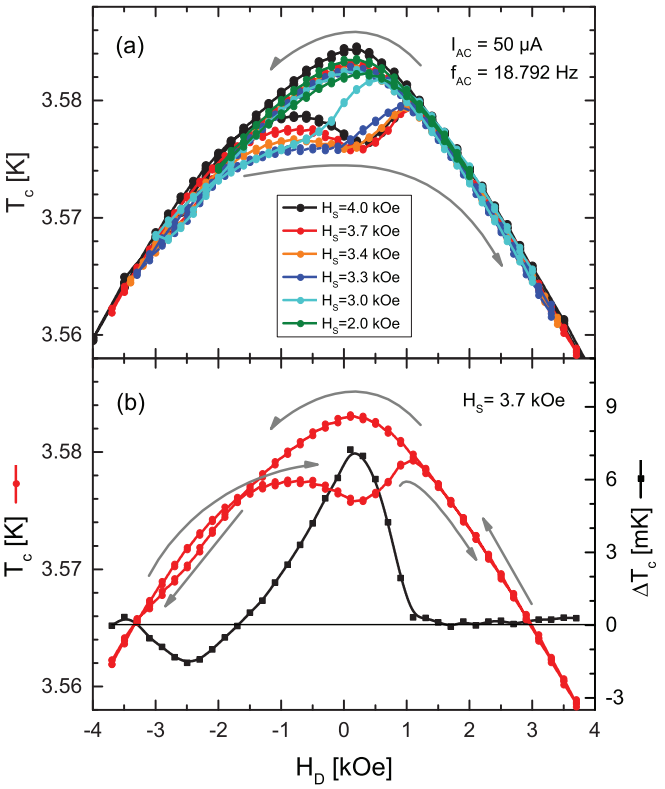

FIG. 3. (a) Superconducting transition temperature, T_c as a function of the applied detection field, H_D, for different width of the hysteresis loops, H_S. The transition temperature has been measured and plotted both for an increasing temperature and a decreasing temperature sweep (slightly higher and lower T_c, respectively). (b) Minor loop results for T_c and ΔT_c for $H_S = 3.7$ kOe, where ΔT_c is the difference in T_c between decreasing and increasing H_D. For a detailed discussion of the results for ΔT_c, see Sec. III C. The solid lines are guide to the eye, the arrows indicate the sweep direction of H_D.

significant change of the hysteretic behavior is observed for $H_S \geqslant 4.0$ kOe.

In Fig. 3(a) a selection of critical temperature data measured in minor loops for $H_S = 2.0$ to 4.0 kOe is shown. For better visibility, Fig. 3(b) shows a single minor loop for $H_S = 3.7$ kOe. The black squares show the calculated size of the spin-valve effect, $\Delta T_c(H_D) = T_c$ (decreasing H_D) $- T_c$ (increasing H_D). The solid lines are guide to the eye. In addition to the positive ΔT_c obtained around zero field, at fields between -3.2 and -1.7 kOe a negative effect is observed. We attribute this effect to an inverse conventional spin-valve effect, as discussed in more detail in Sec. III C.

The dependence of ΔT_c as a function of H_D and H_S is shown in Fig. 4(a). The constant small temperature offset between the data for increasing and decreasing H_D for $H_S =$ 3.0 kOe [see Fig. 3(a) and Appendix D] has been corrected in all calculations of ΔT_c (see Appendix D for details). For decreasing H_S the effect shifts to increasingly negative values of H_D and decreases in size. The fact that for $H_S > 4$ kOe the effect becomes fairly independent of H_S, indicates that all magnetic transitions, necessary to occur for the effect to establish, are within this range of fields. In more detail, a critical range of H_S (in the further text denoted as the breakdown range) can be identified, over which the size of the effect breaks down, from its maximum value to below 2 mK.

Figure 4(b) shows the data for two distinct detection fields, which are most interesting for application: The maximum of the effect occurs at $H_D = 0.2$ kOe, for $H_D = 0$ kOe the system represents a superconducting MRAM element, which needs magnetic fields only to set the state (by applying $\pm H_S$, respectively) and neither for its storage nor for its readout. The breakdown range can also be identified from this representation of the data (indicated as gray shaded region).

B. SQUID magnetometry

To identify the magnetic transition correlated with the breakdown range above $H_S = 3$ kOe, we performed superconducting quantum interference device (SQUID) magnetometry at $T = 10$ K (after cooling and subsequent magnetic training in a field of ± 50 kOe applied parallel to the film plane) for a set of different H_S, ranging from the full loop with $H_S = 50$ kOe to minor loops corresponding to almost absent SSV effect with $H_S < 3$ kOe. The magnetic moments obtained are given in emu according to the cgs-emu system [64], in which 1 emu $\widehat{=}$ 10^{-3} Am^2 in SI units.

Figure 5(a) shows the obtained magnetic moment hysteresis loops, the small anomalies around zero field are artifacts from changing the polarity of the magnet. Basically, the minor loops behave as expected, however, the deviation between $H_D = -3.5$ to -1 kOe for decreasing fields are unexpected, because all loops seem to start from positive saturation. This indicates, that, even for the loop with $H_S = 6$ kOe, the magnetization is not completely saturated for $H_D = +H_S$. This deviation is strongest between $H_S = 6$ and 4 kOe, where there is almost no difference in the size of the triplet SSV effect. Thus, this possible influence on ΔT_c is negligible.

When H_S is decreased, the branch of the hysteresis loop for increasing H_D shifts to smaller detection fields. This shift has also been observed for the triplet spin-valve effect [see the course of the ridge of ΔT_c in Fig. 4(a)].

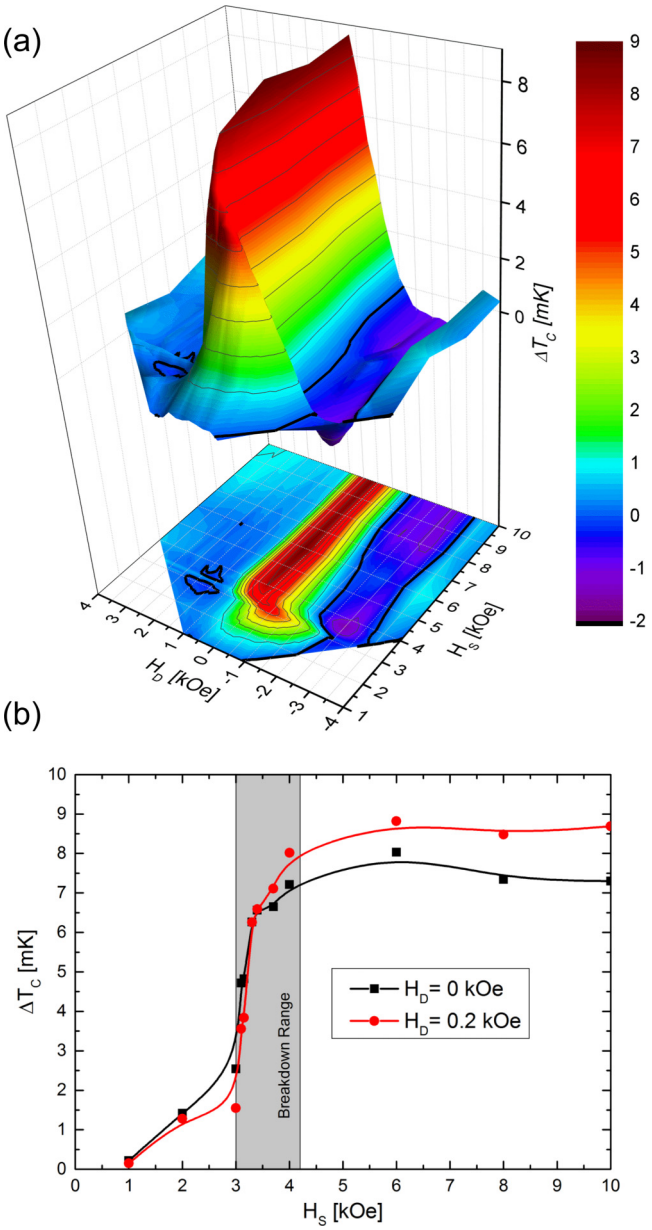

FIG. 4. (a) Size of the triplet SSV effect, i.e., the difference in transition temperature, ΔT_c, between T_c obtained for decreasing and increasing detection field, H_D, as a function of H_D, and the reversal field, H_S. The difference was calculated between the average of T_c obtained from R(T) transition curves for increasing and decreasing temperature. For better visibility, the dependence of the triplet SSV effect is also plotted as projection to the H_D-H_S plane. The bold lines in both representations represent $\Delta T_c = 0$. (b) Triplet SSV effect, ΔT_c, as a function of H_S for two distinct values of H_D most promising for application, i.e., at 0.2 kOe (red), where the effect is most pronounced, and at zero field (black), representing a superconducting MRAM element (for details see the text). The solid lines are guide to the eye, the breakdown range (for details see the text) is indicated in gray.

Since all obtained loops are already more or less saturated at the positive breakdown field range for increasing H_D,

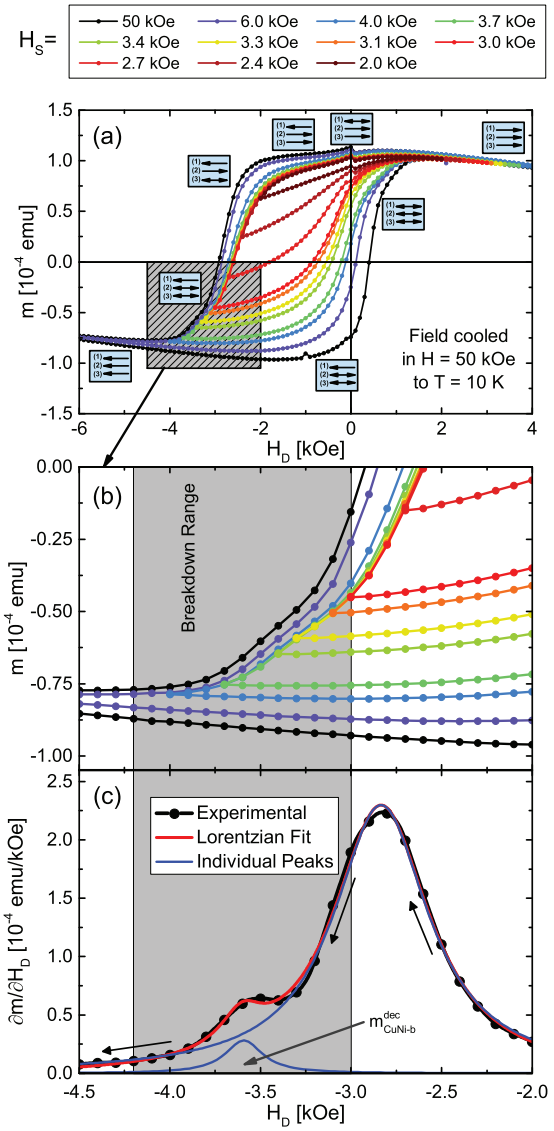

FIG. 5. (a) Magnetic moment hysteresis loops obtained by SQUID magnetometry for different sweep widths, H_S, after cooling to 10 K in a field of 50 kOe applied parallel to the film plane. The small spikes at zero field are artifacts from switching the polarity of the magnet. The pictograms indicate the respective magnetization direction of (1) the top $Cu_{41}Ni_{59}$, (2) the bottom $Cu_{41}Ni_{59}$, and (3) the Co layer. Double-sided arrows indicate a multidomain state or a rotating magnetization. (b) Magnification of the vicinity of the field region, at which the magnetic transition correlated with the triplet SSV effect is expected [see Fig. 4(b)], indicated in gray. An additional structure beside the large Co transition is visible in the breakdown range. Solid lines in (a) and (b) are guide to the eye. (c) Field derivative of the magnetic moment for $H_S = 50$ kOe (black dots). The black solid line is guide to the eye. The arrows indicate the field sweep direction. The constant contributions to the derivative from diamagnetic and paramagnetic (linear) signals, as obtained from high H_D data, have been subtracted (for details see Appendix B). Two different magnetic transitions are clearly distinguishable and fitted by a superposition of two Lorentzian peaks (red). The blue lines show the two individual peaks. The breakdown range coincides with the minor magnetic transition (the area of the peak is a measure for the magnetic moment associated with the transition of the bottom $Cu_{41}Ni_{59}$ layer at decreasing field, $m^{\mathrm{dec}}_{\mathrm{CuNi}\text{-}b}$). For details see the text.

the magnetic transition, which is essential to enable the triplet SSV effect and which fails to be passed for H_S below the breakdown range, is expected to occur in the negative breakdown field range for decreasing H_D [see the gray shaded range in Fig. 5(b)].

In this range, an additional structure in the major magnetic transition (associated predominantly with the Co layer, as discussed below) is observed. In the following we will refer to this structure as the minor magnetic transition.

Apparently, if H_S becomes too small to enable the minor magnetic transition to occur, ΔT_c decreases severely. To verify this observation, we calculated field derivatives of the hysteresis loop with $H_S = 50$ kOe [see Fig. 5(c), black dots/line] for decreasing H_D. The two magnetic transitions are clearly distinguishable. To extract the two individual transitions, we fitted the curve as a superposition of two Lorentzian peaks (this approach is the field derivative analog to the description of magnetic hysteresis loops by the model of Geiler *et al.* [66]), given as red solid line. The fits describe the field derivate reasonably well and can be split into the two constituent contributions (blue lines). The breakdown range coincides with the range of the minor magnetic transition, giving evidence for the direct correlation of the transition with the triplet SSV effect.

To discuss the observations in more detail, a knowledge of the magnetic behavior of the different layers is necessary. However, the magnetic transition of the top $Cu_{41}Ni_{59}$ layer for decreasing field is veiled by an artifact and, for increasing field, all the transitions are overlapping, so that the magnetic transitions of the $Cu_{41}Ni_{59}$ layers cannot unambiguously be separated from the total hysteresis curve. For magnetic hysteresis loops for samples of the same sample series with a larger thickness of the $Cu_{41}Ni_{59}$ layers, see Fig. 2 of Ref. [57] and Fig. 9.4 of Ref. [67]. Similar to the present work, the transitions for decreasing field are clearly distinguishable, whereas for increasing field only two transitions are visible in these works.

We determined the saturation magnetic moments of the two magnetic transitions for decreasing H_D, which could be separated from the field derivative of the $m(H_D)$ curve (for $H_S = 50$ kOe) shown in Fig. 5(c). Details of the evaluation are given in Appendix B. The obtained saturation magnetic moments of the major and minor magnetic transitions can be related to the Co and the bottom $Cu_{41}Ni_{59}$ layer, respectively.

In the breakdown range of decreased sweep width H_S, the magnetic moment reversed in the minor magnetic transition becomes smaller, i.e., the magnetization reversal of the bottom $Cu_{41}Ni_{59}$ layer becomes stepwise more and more incomplete.

Before we discuss the obtained magnetic hysteresis loops in more detail, further properties of the magnetic layers of the sample will be discussed. For not exchange biased thin $Cu_{41}Ni_{59}$ films and the range of thicknesses present in the sample series of the current study, a magnetic easy axis perpendicular to the film plane is expected [68–70]. The magnetic easy axis of thin Co films of thickness comparable to the one in the present sample is in the film plane [71–75].

For Co/CoO bilayers it has been observed by polarized neutron reflectometry (PNR) that for magnetic fields applied parallel to the film plane, the first magnetization reversal after field cooling occurs via nucleation and propagation of

domain walls. The second and all subsequent reversals are characterized by in-plane domain rotation [76–78]. For films thinner than the domain wall thickness expected for cobalt (50 nm), the magnetic domains in the Co layer can be assumed to extend over the entire thickness of the film [78]. This is valid for all Co films of the cited literature (3–40 nm) and the present paper (4.6 nm).

During the first magnetization reversal, interfacial magnetic domains are generated at the Co/CoO interface, which are preserved even in saturation [77,79]. These domains are intimately related to the antiferromagnetic domain state (see Sec. 3.13 of Ref. [58]) and serve as seeds for domain nucleation in subsequent magnetization reversals [77].

In contrast to the cited literature, in the present paper, the CoO_x layer is much thicker (16.0 nm compared to 2.0–4.5 nm). The domain state model predicts a strong change of the exchange bias field for very thin antiferromagnetic layers [80] (experimentally observed in $Co/Co_{1-\delta}O$ [81]). Moreover, the development of an antiferromagnetic exchange spring is possible [82] and can also be affected by the thickness.

However, the training effects observed in subsequent magnetic hysteresis curves of Co/CoO bilayers of thickness 13.9 nm/3.3 nm [78] and 13.0 nm/4.5 nm [79] (recorded at $T = 10$ K and 30 K, respectively) are similar to those of a sample with Co/CoO_x thicknesses 5 nm/19 nm (recorded at $T = 10$ K) from the same sample series as the sample investigated in the present work (see Fig. 2 of Ref. [57]). While the first magnetization reversal shows a sharp change in magnetization, the subsequent reversals show a more rounded shape. The underlying mechanism of this type of training effect is an irreversible change of the domain state of the antiferromagnet from an initial single-domain state after field cooling to a multidomain state after the first reversal. In addition to the resulting change of reversal mechanism and the creation of interfacial domains, discussed above, this multidomain state leads to a reduction of the exchange bias field and the coercivity, due to the lateral distribution of anisotropy in the antiferromagnetic layer. For a detailed discussion of these effects, see p. 162 of Ref. [58].

First PNR experiments performed on a sample from the same series (directly adjacent to the sample of the present work) confirm the magnetization reversal by in-plane domain rotation in the trained state. The properties of the $Cu_{41}Ni_{59}$ layers cannot be obtained from the PNR measurements due to their low magnetic contrast.

We interpret the obtained SQUID data in the following model. For high positive magnetic fields all magnetic layers are in the saturated state. For decreasing field, this remains valid until H_D approaches zero. When the top $Cu_{41}Ni_{59}$ layer changes its magnetization direction, this leads to a region at $H_D < 0$, where its magnetization direction is antiparallel to the exchange-biased bottom $Cu_{41}Ni_{59}$ layer. Then, between $H_S \approx 1.8$ and ≈ 4 kOe, the exchange biased Co (major transition) and bottom $Cu_{41}Ni_{59}$layer (minor transition) reverse their magnetization direction, leading to the negative saturated state.

The interpretation of the results for increasing H_D is difficult due to the lack of clear structures in the curve. Thus, the interpretation partially relies on the superconducting results, which are discussed in the framework of the magnetic data in the following section. While the deduction of the magnetic configuration solely based on the magnetic data and subsequent interpretation of the superconducting results in this framework would be preferable, such approach is impossible due to the weak signal from the $Cu_{41}Ni_{59}$ (on the background of the strong Co signal). This is, however, an intrinsic property of the system and, thus, unavoidable. Moreover, the magnetic properties in the superconducting state might be different to the ones measured in the normal conducting state, however, in the superconducting state an additional huge background from the vortex phase is present, which is additionally obstructing the interpretation.

We attribute the first (major) transition in this sweep direction to the Co and $Cu_{41}Ni_{59}$ layer, which are coupled via the CoO_x, and the second (minor) transition to the top $Cu_{41}Ni_{59}$ layer (for examples of field derivatives of the magnetic moment for this sweep direction, see Sec. III C and Appendix D). From the superconducting transport results, we expect the coupling to induce noncollinearities extending over the thickness of the bottom $Cu_{41}Ni_{59}$ layer, e.g., in the form of an exchange spring (see Ref. [83] and p. 279 of Ref. [84]). The competition between the intrinsic perpendicular anisotropy of $Cu_{41}Ni_{59}$ films (see above) and the in-plane anisotropy, which can be induced by the coupling to the CoOx and the Co layer, might lead to such noncollinearities. These noncollinearities generate spin-projection one-triplet pairing components [46,85–88], yielding a reduction of T_c. A lateral noncollinear distribution of domains, which extend over the entire thickness of the layer and are separated by Néel walls, are not expected to generate the spin-projection one-triplet pairing wave function [89] and, thus, should not produce a triplet SSV effect. Instead, even an increase of T_c can be found [90].

This model requires an interlayer coupling [91–97] of the Co layer via the CoO_x layer to the bottom $Cu_{41}Ni_{59}$ layer. Interlayer coupling has been observed, e.g., between a Co and a $Ni_{80}Fe_{20}$ layer across an antiferromagnetic oxide (NiO) [96] over large thicknesses (up to 25 nm) and between a Co and a $Cu_{45}Ni_{55}$ layer across few nanometers of an antiferromagnetic metal (FeMn) [97]. Due to the strong dependence of such coupling on local anisotropies and domain structures, the noncollinearity of the magnetic moments in the bottom $Cu_{41}Ni_{59}$ layer possibly varies in space (for a detailed discussion see Appendix C).

While according to the domain state model, the exchange bias field (the shift of the hysteresis loop on the field axis) of the ferromagnetic layer is determined only by the irreversible part of the (normalized) domain state magnetization of the interface layer of the antiferromagnet adjacent to the F layer (see Eq. (4) of Ref. [80]), the details of the coupling mechanism, which correlates the Co and bottom $Cu_{41}Ni_{59}$ layer, might possibly depend on the total (normalized) domain state magnetization of the antiferromagnet. This magnetization is not constant during field reversal (see Figs. 4 and 5 of Ref. [80]) and hard to isolate from a conventional hysteresis loop, as here the sum of the magnetic moments of the F layer, the volume contribution of the antiferromagnet and its interface layer is measured (see Figs. 4 and 5 of Ref. [80] for a calculation of the separate contributions).

Apparently, the coupling between the Co and bottom $Cu_{41}Ni_{59}$ is different for the two magnetization reversals in the present study, as the superconducting properties are

fundamentally different. While for the reversal occurring at decreasing H_D, no evidence of a triplet SSV effect and, thus, no evidence for noncollinear magnetizations in the bottom $Cu_{41}Ni_{59}$ has been observed, for the opposite sweep, a clear reduction of T_c by the triplet SSV effect has been found.

One possible model would be that the coupling between the two ferromagnetic layers is weaker in the reversal at decreasing H_D, so that the reversal occurs without inducing noncollinearities into the magnetic moments of the bottom $Cu_{41}Ni_{59}$ layer, while for increasing H_D the coupling might be stronger and, thus, the domain state rotation of the Co induces noncollinearities into the bottom $Cu_{41}Ni_{59}$ layer, e.g., in the form of an exchange spring. An evidence for this model would be that, while for decreasing H_D there is a distinct peak observable for the reversal of the bottom $Cu_{41}Ni_{59}$ layer, for increasing H_D it is so strongly correlated to the Co reversal, that it is not distinguishable.

C. Correlation of results

1. Qualitative correlation

In this section, we will try to qualitatively relate the observed $T_c(H_D)$ behavior to the magnetic model discussed in the section above. For saturated magnetic states, i.e., for decreasing fields above ≈ 0 and below ≈ -4 kOe and increasing fields below ≈ -3 and above ≈ 1 kOe, the $T_c(H_D)$ data follow a Ginzburg-Landau-like behavior (see Ref. [54] for a detailed discussion of similar data).

In the range of antiparallel alignment of the two $Cu_{41}Ni_{59}$ layers (H_D between ≈ -1.5 and ≈ -3 kOe) an inverse F/S/F SSV effect is observed, which slightly reduces T_c. There are four regions, which could possibly show noncollinear magnetic moments and, thus, triplet SSV effects. However, the magnetic reversal of the top $Cu_{41}Ni_{59}$ layer (around $H_D \approx 0$ and ≈ 1 kOe for decreasing and increasing H_D, respectively), as well as the reversal of the bottom $Cu_{41}Ni_{59}$ layer for decreasing field (around 4 kOe) is not leading to a reduction of T_c.

Although the dirty limit theory predicts a contribution of the spin-projection one triplet component to the superconducting T_c of a F/S/F type SSV, a triplet SSV effect is absent [18,20]. It is only predicted for the clean limit of the magnetic material [20] for which it is also observed experimentally [52,56]. Our samples are, however, in the intermediate state between dirty and clean limit [8,9]. Due to the absence of visible triplet effect at the Co reversal for decreasing H_D, we conclude that there are no noncollinearities induced into the bottom $Cu_{41}Ni_{59}$ layer by this magnetic reversal.

The fourth possible region for noncollinear magnetic moments is the reversal of the bottom $Cu_{41}Ni_{59}$ layer at increasing field. However, as discussed above, the magnetic transition is coupled to that one of the Co layer. The interlayer coupling induces noncollinearities (e.g., in the form of an exchange spring) into the bottom $Cu_{41}Ni_{59}$ layer, resulting in the observed reduction of T_c. Again, this is not a F/S/F triplet SSV effect (which is apparently absent in the present sample, see above for a discussion), but a triplet SSV effect arising from internal noncollinearities in the bottom $Cu_{41}Ni_{59}$ layer alone.

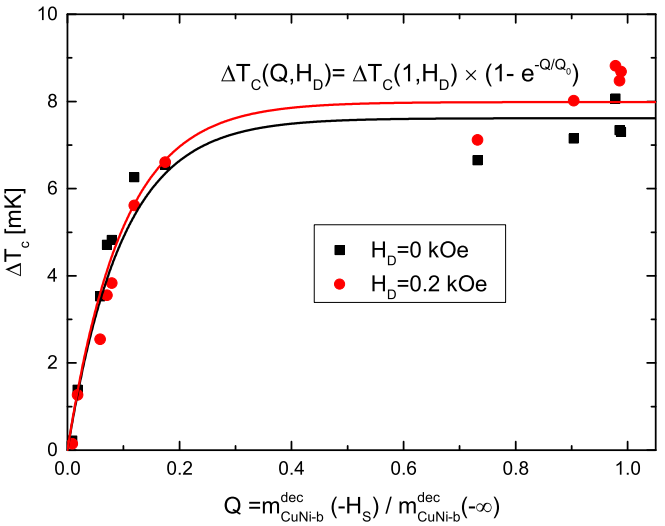

FIG. 6. Triplet SSV effect, ΔT_c, as a function of the fraction of magnetic moment in the minor magnetic transition, turned at the negative reversal field, $-H_S$. The solid lines gives an empirical exponential fit to the data according to Eq. (3). For details and the obtained fit parameters, see the text.

There is a slight asymmetry in the $T_c(H_D)$ behavior with respect to $H_D = 0$, even considering the aforementioned effects. The reason is unknown, however, there appears to be an increase of T_c at negative fields below -1.7 kOe. While domain structures enhanced T_c has been reported in literature [90,98], neither the bottom $Cu_{41}Ni_{59}$ nor the top $Cu_{41}Ni_{59}$ layer are in a multidomain state in this range and earlier measurements on $Nb/Cu_{41}Ni_{59}$ bilayers have shown no evidence of such effects [99].

2. Quantitative correlation

To quantitatively relate the dependence of ΔT_c on H_S [see Fig. 4(b)] to the minor magnetic transition (the magnetic transition of the bottom $Cu_{41}Ni_{59}$ layer at decreasing field), we plot ΔT_c as a function of Q (see Fig. 6), defined as

$$Q(H_S) = \frac{m^{\mathrm{dec}}_{\mathrm{CuNi}\text{-}b}(-H_S)}{m^{\mathrm{dec}}_{\mathrm{CuNi}\text{-}b}(-\infty)} \tag{1}$$

representing the fraction of magnetic moment of the minor magnetic transition turned from positive to negative field direction at $H_D = -H_S$. The magnetic moment is obtained by

$$m^{\mathrm{dec}}_{\mathrm{CuNi}\text{-}b}(H'_D) = \int_{H'_D}^{\infty} \frac{\partial m^{\mathrm{dec}}_{\mathrm{CuNi}\text{-}b}}{\partial H_D} \mathrm{d}H_D \tag{2}$$

with $\frac{\partial m^{\mathrm{dec}}_{\mathrm{CuNi}\text{-}b}}{\partial H_D}$ as obtained according to Sec. III B, see Fig. 5(c).

The dependence $\Delta T_c(Q)$ in Fig. 6 is clearly nonlinear and can empirically be fitted by an exponentially saturating behavior

$$\Delta T_c(Q, H_D) = \Delta T_c(1, H_D)(1 - e^{-\frac{Q}{Q_0}}) \tag{3}$$

with the fit parameters $\Delta T_c(1, H_D)$ and $Q_0 \ll 1$ (shared among both fits). We obtain $Q_0 = (9.7 \pm 0.8) \times 10^{-2}$, $\Delta T_c(1,0\ \mathrm{kOe}) = (7.6 \pm 0.2)$ mK, and $\Delta T_c(1,0.2\ \mathrm{kOe}) = (8.0 \pm 0.3)$ mK, respectively. The parameter $\Delta T_c(1, H_D)$ is

the triplet SSV effect obtainable at H_D for the minor magnetic transition being entirely completed.

The reason for the reduction of the triplet SSV effect, if H_S only enables an incomplete minor magnetic transition is, that the amount of noncollinear magnetic moment achievable for increasing H_D (magnetic moments turning from negative to positive field direction) is obviously limited by the magnetic moments turned from positive to negative field direction previously.

If it would be possible to separate the contribution of the $Cu_{41}Ni_{59}$ bottom layer for increasing field, $m^{\text{inc}}_{\text{CuNi-}b}$, from the total $m(H_D)$ curve for $Q = 1$ (as, e.g., the case for $H_S = 6$, 8, and 10 kOe, see Fig. 5), the function $\Delta T_c(1, H_D)$ could be directly determined. It should depend on the noncollinearity of the local magnetic moments in the bottom $Cu_{41}Ni_{59}$ layer at H_D.

In a first approximation, the exchange-spring-like magnetic order, assumed to be present in the bottom $Cu_{41}Ni_{59}$ layer during reversal, can be simplified assuming the most rigid end of the spring to start rotating at the coercive field, where the rotation of the least rigid part of the spring has already finished. Figuratively, this reflects a fan of magnetic moments being opened entirely and subsequently closed to the other side.

In such an approximation, the projection of the magnetic moment of the bottom $Cu_{41}Ni_{59}$ layer on H_D (detected by the SQUID magnetometry) is correlated to the noncollinearity in the magnetic moments (the opening angle of the fan). The magnetic moment projection becomes zero for the completely fanned out state and approaches the saturation magnetization for the fan of magnetic moments being closed. A more direct measure of the magnetic noncollinearities is the field derivative, $\partial m^{\text{inc}}_{\text{CuNi-}b}/\partial H_D$, which is maximal and zero in the completely fanned out and closed state, respectively. While there is no such simple correlation for an arbitrary exchange spring, we nevertheless consider such a field derivative of the projection of magnetic moment as reasonable measure of the noncollinearity.

Since the maximum of the triplet SSV effect is expected for the maximal magnetic non-collinearity [19,21], in this approximation, we obtain

$$\Delta T_c(1, H_D) = \Delta T_c(1, H_D^*)\, f\left(\left.\frac{\partial m^{\text{inc}}_{\text{CuNi-}b}}{\partial H_D}\right|_{H_D} \right) \tag{4}$$

with f an empirical function satisfying

$$f\left(\left.\frac{\partial m^{\text{inc}}_{\text{CuNi-}b}}{\partial H_D}\right|_{H_D^*} \right) = 1$$
$$f\left(\left.\frac{\partial m^{\text{inc}}_{\text{CuNi-}b}}{\partial H_D}\right|_{\pm\infty} \right) = 0 \tag{5}$$

with H_D^* the field realizing the maximum of $\frac{\partial m^{\text{inc}}_{\text{CuNi-}b}}{\partial H_D}$.

Unfortunately, we did not succeed in separating $m^{\text{inc}}_{\text{CuNi-}b}$ from the total magnetization curve. The reason is that apparently the magnetic transition does not follow the Geiler model [66]. However, as discussed in Sec. III B it is assumed that the magnetic behavior of the Co layer drives the noncollinearities in the bottom $Cu_{41}Ni_{59}$ layer, yielding the triplet SSV effect. Since the saturation magnetic moment expected for the Co layer is about a factor of 10 larger than that one of the $Cu_{41}Ni_{59}$ layers (see Appendix B) we try to relate the derivative $\frac{\partial m}{\partial H_D}$ of the total hysteresis curve for increasing H_D to $\Delta T_c(H_D)$, which are both shown in Fig. 7 for $H_S = 4.0$ kOe. For further plots of this type for different H_S see Appendix D. Please note that constant paramagnetic, diamagnetic or antiferromagnetic contributions are not subtracted, but negligible, because they are of the order of 10^{-6} emu/kOe.

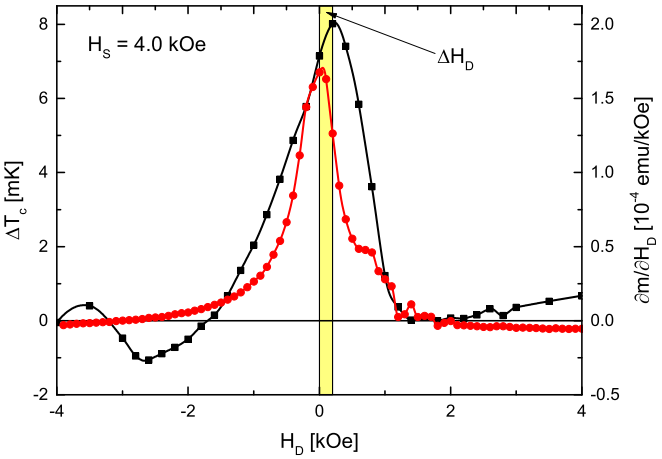

FIG. 7. Superconducting spin-valve effect, ΔT_c (black squares), and total magnetic moment field derivative for increasing H_D, $\frac{\partial m}{\partial H_D}$ (red dots) as a function of the applied field, H_D, at $H_S = 4$ kOe. The yellow shaded range indicate the shift between the maximum of the derivative and that one of the SSV effect, ΔH_D. The solid lines are guide to the eye.

The basic overall shapes of $\frac{\partial m}{\partial H_D}$ and $\Delta T_c(H_D)$ appear to be similar, except in the field range of $\Delta T_c < 0$, which is governed by the inverse F/S/F SSV effect (as discussed in Sec. III C 1). Especially, the field range of nonvanishing $\frac{\partial m}{\partial H_D}$ coincides with the range of nonzero $\Delta T_c(H_D)$. This fact strengthens our assumption that the noncollinearities are induced by an interaction of the $Cu_{41}Ni_{59}$ layer with the Co layer.

The saturation magnetic moment obtained from an estimation of the peak area of the major transition for increasing H_D is close to the one expected for the Co layer (see Appendix B). An estimation of the saturation magnetic moment for the visible minor transition was not possible with reasonable accuracy.

Obviously, the magnetic transition related to the structure at the end of the sweep in Fig. 7 cannot alone be responsible for the occurrence of the triplet SSV effect, because the range does not match. Thus, we conclude the minor transition to be mainly containing the magnetic moment of the top $Cu_{41}Ni_{59}$ layer. Consequently, we conclude that the magnetic transition of the bottom $Cu_{41}Ni_{59}$ layer is correlated with that one of the Co layer. However, the correlation appears to be shifted on the field scale by $\Delta H_D = H_D^* - H_{D,\max}$, as the maximum of the SSV effect at $H_{D,\max}$ and the derivative of magnetic moment at H_D^* do not match. A possible reason is the larger intrinsic magnetic hardness of $Cu_{41}Ni_{59}$ compared to Co (harder materials exhibit a larger width of the hysteresis loop than softer ones [84]). Further evidence for this assumption is given from the change of the field position of the maxima for decreasing H_S. The maximum of the effect shifts stronger than the maximum of the derivative (see Figs. 11 and 12 in Appendix D), which is

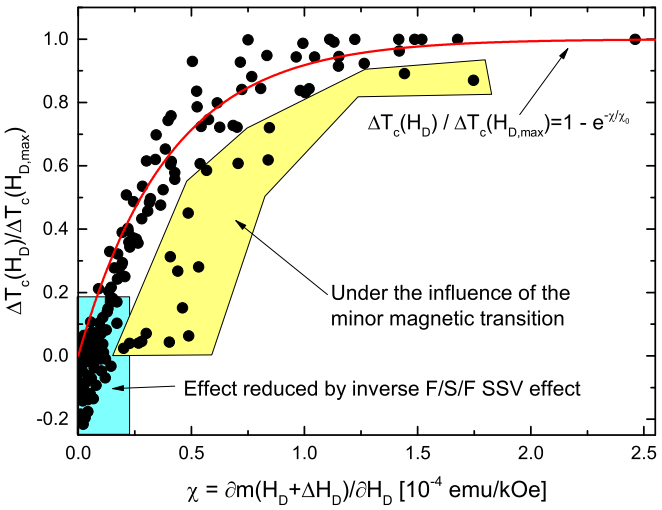

FIG. 8. Superconducting spin-valve effect, $\Delta T_c(H_D)$, normalized to the maximum value $\Delta T_c(H_{D,\max})$ for the respective H_S, as a function of the field derivative $\chi = \frac{\partial m(H_D+\Delta H_D)}{\partial H_D}$ for increasing H_D (for a plot with color indicated sweep widths, H_S, see Appendix E). Here, ΔH_D is the field shift between the maximum of the derivative and the maximum of the effect. The red line shows the empirical correlation, according to Eq. (7) with $\chi_0 = 4.0 \times 10^{-5}$ emu/kOe. For the fit of χ_0, the data inside the blue (effect suppressed by inverse F/S/F SSV effect) and yellow range (increased χ due to minor magnetic transition) have been neglected.

expected considering that the $Cu_{41}Ni_{59}$ layer (yielding the SSV effect) enters a minor loop already at higher H_S than the Co layer (dominating the derivative). See Ref. [100] or Figs. 5(a), 11, and 12 of the present paper for examples of minor loops.

Since the derivative $\chi = \partial m(H_D + \Delta H_D)/\partial H_D$ seems to be closely related to $\Delta T_c(H_D)$, we plotted $\Delta T_c(H_D)/\Delta T_c(H_{D,\max})$ as a function of χ for several H_S in Fig. 8. A plot, indicating the different H_S for the data points, is given in Appendix E.

To be able to isolate the dependence of ΔT_c on H_D, it is necessary to get rid of the influence of the varying H_S and, thus, the Q dependence. According to Eq. (3), such a Q-independent quantity can be obtained by normalizing $\Delta T_c(Q, H_D)$ by its maximum $\Delta T_c(Q, H_{D,\max})$ for the same Q, yielding

$$\frac{\Delta T_c(Q, H_D)}{\Delta T_c(Q, H_{D,\max})} = \frac{\Delta T_c(1, H_D)}{\Delta T_c(1, H_{D,\max})} \tag{6}$$

and, thus, independent of Q.

The figure indicates that such a relation, independent of Q, exists and can be described by

$$\frac{\Delta T_c(1, H_D)}{\Delta T_c(1, H_{D,\max})} = f(\chi) = 1 - e^{-\chi/\chi_0}. \tag{7}$$

In more detail, the outliers from the majority of the data points toward the right side and toward too small effects can be assigned to fields under the influence of the minor magnetic transition (see yellow shaded range), which is not driving the effect, and the inverse F/S/F SSV effect (see blue shaded range), respectively. If we exclude those data points from the fit according to Eq. (7), we obtain $\chi_0 = 4.0 \times 10^{-5}$ emu/kOe.

Comparing the obtained expression with Eq. (4), it is $\Delta T_c(1, H_D^*)$ substituted by $\Delta T_c(1, H_{D,\max})$. Moreover, we evaluate the field derivative corresponding to $\Delta T_c(1, H_D)$ at $H_D + \Delta H$. The normalization condition given by Eq. (5) is fulfilled by $f(\chi)$, since the derivative is correspondingly taken at $H_{D,\max} + \Delta H = H_D^*$, as long as $\chi(H_D^*) \gg \chi_0$. The evaluation of the derivative and the SSV effect being shifted on the field scale by ΔH_D is a consequence of the field shift between the magnetic transition of the Co and the bottom $Cu_{41}Ni_{59}$ layer. The second condition given by Eq. (5) is also fulfilled, since $\chi(H_D = \pm\infty) = 0$ and, according to Eq. (7), $f(\chi = 0) = 0$.

D. Switching properties

Although the value of ΔT_c generated by the triplet SSV effect is small, it is nevertheless possible to operate the device with full switching. This means that, at a given temperature, the sample is completely superconducting or normal conducting depending on the magnetic history. To achieve full switching it is necessary that ΔT_c is larger than the width of the superconducting R(T) transition. Even for an optimized set of operation parameters, H_D, H_S, and T, the size of the effect, ΔT_c, is considerably smaller than the transition width of approximately 60 mK (see Fig. 9). However, the transition width strongly depends on the transport current used for detecting the resistance.

The transitions at different transport currents, I, are plotted in Fig. 9(a). In contrast to all measurements reported so far in the present paper, all measurements with increased transport current are performed with dc current, because for unknown reasons (to be investigated) the narrowing of the transition width for increased currents is very limited under ac conditions, even at the very small frequencies used. All dc resistances given in Figs. 9 and 10 are measured using the same four-point probe setup as the ac resistances presented above. After stabilizing each temperature for 30 s, the measured resistance is averaged over ten measurements performed over a period of 30 s to verify stability of the resistance. The resistance is measured with both polarities to get rid of possible thermovoltages, the temperature has been varied from higher to lower ones.

At currents above 200 μA the transition narrows considerably and, approaching a critical value around 450–500 μA, becomes steplike on a single-mK scale. A possible reason for the narrowing could be avalanchelike flux flow [101] or an instability of the flux line motion in the resistive mixed state [102–104]. The size of the triplet SSV effect, ΔT_c, has been checked to be fairly independent of the transport current.

Heating effects seem not to dominate the transition narrowing. There are no signatures of self-heating hot spots [105–108] in the transition curves up to $I_{DC} = 425$ μA although the transition width is already considerably reduced. Moreover, if heating effects would be of major importance for a transition width reduction, due to scaling of the heating power with the resistance of the sample, the R(T) curve would be asymmetric, which is not the case up to $I_{DC} = 425$ μA.

To clarify the transition sharpening mechanism, an extensive study of voltage-current [V(I)] characteristics according to Refs. [102–104] has to be conducted and analyzed. This is,

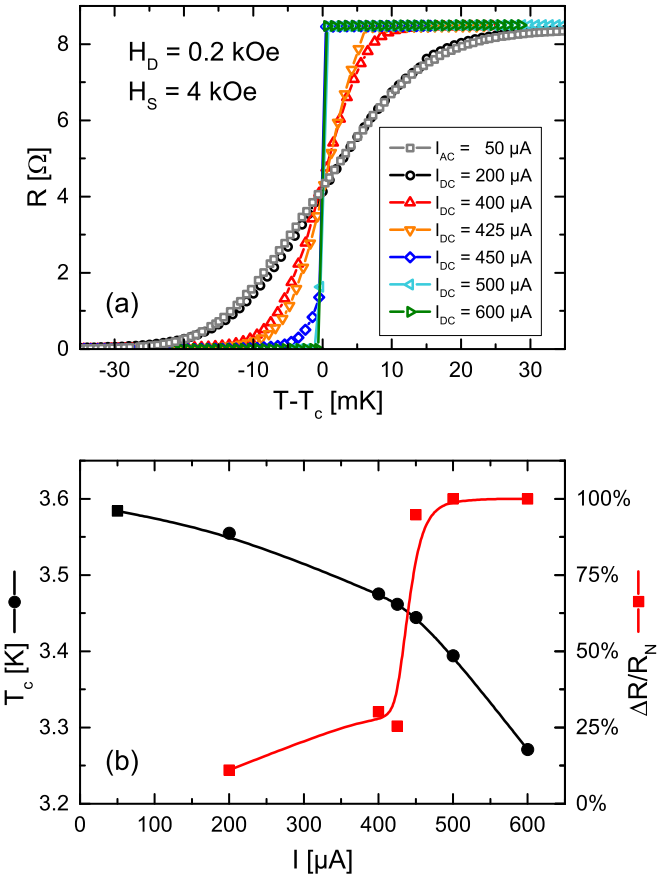

FIG. 9. (a) Superconducting transitions at $H_D = 0.2$ kOe and $H_S = 4$ kOe and various transport currents, I, plotted as a function of the temperature relative to the transition temperature, T_c. All transitions plotted have been recorded after increasing the applied field from $-H_S$ to H_D and at decreasing T. There is an obvious sharpening of the transition above $I_{DC} = 200$ μA, yielding a transition width of less than 1 mK for $I_{DC} = 600$ μA. (b) Corresponding superconducting transition temperature (left scale, black symbols and line) and switching capability, $\Delta R/R_N$ (for a definition, see the text), normalized to the normal state resistance (right scale, red symbols and line) as a function of the applied current. Please note that the point at $I = 50$ μA (black square) is obtained using ac current, while all other data points are obtained by measurements with dc current. The solid lines are guides to the eye.

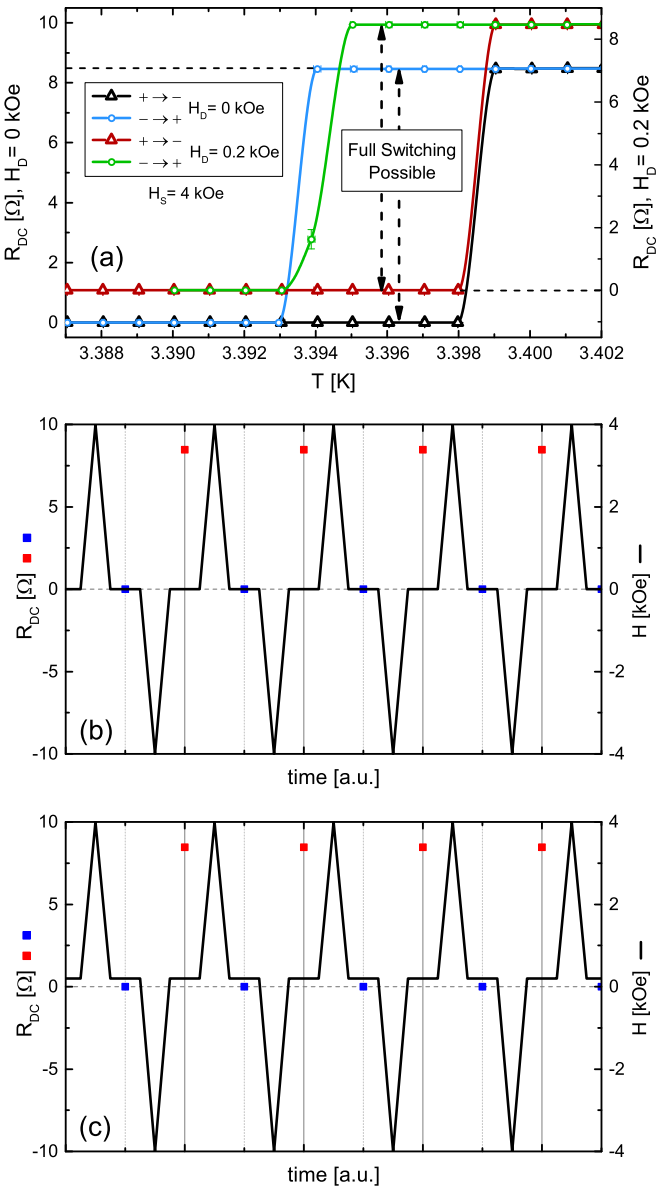

FIG. 10. (a) Superconducting R(T) transitions measured at $H_D = 0$ and 0.2 kOe for decreasing and increasing H_D (black triangles/blue circles and brown triangles/green circles, respectively). The sweep width, H_S, and the applied dc current I_{DC} have been chosen as 4 kOe and 500 μA, respectively. As indicated, full switching from the superconducting to the normal conducting state is possible. (b), (c) Demonstration of the switching between the normal state (red squares) and the superconducting state (blue squares) at $T = 3.397$ K for $H_D = 0$ and 0.2 kOe, respectively (other parameters as above). The solid curve illustrates the magnetic field applied for the switching.

however, beyond the scope of the present paper. In any case, for an application, lithographic methods would be applied to reduce the size of the MRAM element and, thus, its heating power, however, conserving the necessary current density to activate the transition narrowing mechanism.

Besides the narrowing of the transition, there is also a pair-breaking influence of the increased transport current and, thus, a decrease of T_c. However, the pair-breaking effect of transport currents even up to 600 μA, considerably above the current necessary for a transition width in the single-mK range, does not reduce T_c below the temperature range available by using ^{4}He as cooling agent [see Fig. 9(b)] and is, thus, acceptable from an application point of view.

Moreover, in Fig. 9(b) the resistance change, ΔR (normalized to the normal state resistance, R_N), achievable by switching between the two different magnetic states, is plotted as a function of the transport current. It shows the expected steep increase once the transition width becomes comparable with ΔT_c. The resistance differences ΔR are obtained by measuring transition curves as a function of temperature in both states with the given transport currents and calculating the maximum difference of resistance between both transitions. For high enough currents this difference

becomes R_N, enabling full switching, as shown in Fig. 10(a) for $H_D = 0$ kOe and 0.2 kOe, respectively.

Applying the obtained results to a scenario more close to application, it is possible to demonstrate full switching of the device from the superconducting to the normal conducting state [see Figs. 10(b) and 10(c)], when applying field pulses of $\pm H_S$ (indicated as black lines). This has been achieved at $T = 3.397$ K for $H_D = 0$ kOe and 0.2 kOe (the red and blue resistance values are verified to correspond to the normal conducting and superconducting state, respectively). The switching is also verified to be stable (only a part of the measured switching processes is plotted for the sake of clearness of the figure).

IV. CONCLUSIONS

The $Co/CoO_x/Cu_{41}Ni_{59}/Nb/Cu_{41}Ni_{59}$ thin film heterostructure investigated in the present paper shows a superconducting transition temperature, which depends on the magnetic history. If the field applied parallel to the film plane is increased from negative saturation (relative to the cooling field), the transition temperature is lower than if the field is decreased from positive saturation. We ascribe this finding to the generation of the superconducting long-range odd-in-frequency triplet pairing component with spin-projection one caused by noncollinear magnetic moments in the sample, yielding the so-called triplet superconducting spin-valve effect.

By investigating the superconducting transport and magnetic properties of the sample in minor loops (reducing the absolute value of the applied field at which the direction of change of the field is reversed), we found a correlation of the triplet spin-valve effect to the minor magnetic transition of the exchange biased bottom $Cu_{41}Ni_{59}$ layer at decreasing field, which we were able to separate from the main magnetic hysteresis. Thus, we were able to develop an empirical quantitative description of the dependence of the spin-valve effect on the decisive magnetic operational parameters.

Nevertheless, precise knowledge of the magnetic configuration of the magnetic layers is still missing. It is mostly not possible to obtain detailed information from SQUID magnetometry for the weak $Cu_{41}Ni_{59}$ signal on the background of the strong Co signal. Moreover, also PNR measurements could not resolve the properties of the $Cu_{41}Ni_{59}$ layers. However, all conclusions drawn from the magnetic measurements support the interpretations made.

We demonstrated that the system can serve as a superconducting MRAM element, which is able to operate without requiring an external field for storage or readout of the information, but only to set the logic state. Using increased transport currents the system can, with acceptable pair-breaking influence of the current, be driven into a full-switching mode, in which the two states are completely superconducting and normal conducting, respectively.

In conclusion, the present system can serve as fundamental building block to build up a superconducting MRAM device for application in superconducting spintronics. Thus, the presented triplet spin valve is a superconducting analog to the conventional GMR spin valve for application as MRAM element, however, it has, by its superconducting nature, potential for much higher efficiency.

ACKNOWLEDGMENTS

The authors are grateful to S. Heidemeyer, B. Knoblich, and W. Reiber for the TEM-sample preparation, additionally to W. Reiber for assistance in RBS-measurements, and to D. Vieweg for assistance in magnetic measurements. This work was supported by the Deutsche Forschungsgemeinschaft (DFG) under the Grant No. HO 955/9-1. L.R.T. acknowledges partial support by RFBR (Grant No. 16-02-01171-a), Program of *Competitive Growth* of Kazan Federal University funded by the Russian Government, and R.A.S. Program of *Actual Problems of Low-Temperature Physics*. A.S.S. and R.M. acknowledge support by STCU (Grant No. 5982). The magnetic investigations (H.-A. K.v.N., Yu.K.) were partially supported by the Deutsche Forschungsgemeinschaft (DFG) within the Transregional Collaborative Research Center TRR 80 "From Electronics Correlations to Functionality" (Augsburg-Munich).

APPENDIX A: DIFFERENT SPIN VALVE MECHANISMS IN F/S/F AND FI/S/FI SYSTEMS

Following the pioneering works of Sarma [109], de Gennes [110], Deutscher and Meunier [111], and Hauser [112], recently Li *et al.* [63] prepared a FI/S/FI SSV (using FI = EuS and S = Al), which shows a transition from the entirely normal conducting to the superconducting state, when switched from the parallel to the antiparallel configuration of the magnetizations of the FI layers. Since the device can be either in the high or zero resistance state, even at $H = 0$, it can serve as an MRAM element. Their interpretation is based on the prediction of de Gennes [110] for the exchange field experienced by the conduction electrons and further elaborations of the problem by Kulic and Endres [113].

Thin film FI/S samples in a magnetic field exhibit a spin split quasiparticle excitation spectrum of the superconducting state [114–121], similar to S films [119,122–125]. However, for FI/S films there is an additional contribution to the size of the splitting (for EuS/Al also observed in zero applied field [116]), interpreted as an exchange field induced into the superconductor by the presence of the FI layer. This exchange field decays on a distance of order $\xi_0(T_{c0}) = \hbar v_F/(2\pi k_B T_{c0})$ into the superconductor [126]. The length $\xi_0(T_{c0})$ represents the size of a Cooper pair at $T = T_{c0}$ [127]. Here, k_B is Boltzmann's constant, v_F the Fermi velocity of the S material, and $\hbar = h/2\pi$ with h Planck's constant.

In the theory of Tokuyasu, Sauls, and Rainer [126] the exchange field is a consequence of a boundary condition describing the interaction of electrons that tunnel into the FI and interact with the average exchange field of the local moments. The excess splitting of the quasiparticle density of states results from quasiparticle tunneling into the magnetic insulator and subsequent reflection into the superconductor. In this process the spin vector of the quasiparticles is rotated (the angle of rotation is interpreted as spin mixing angle) and a phase shift occurs between the incident and reflected states, which is not further considered in that theory.

According to Eschrig [128], the reason for the spin rotation is a phase delay between the reflected and the incoming wave at the interface between a superconductor and a ferromagnetic

insulator, which differs for both spin directions. This leads to a spatial modulation of the superconducting singlet pairing component mixed with the spin-projection zero triplet component determined by the spin mixing angle [128] (see Ref. [54] and references therein for a discussion of the different superconducting pairing components).

For a FI/S/FI system, the phase delay and spin-rotation effects increase if the magnetizations of the FI layers are parallel and they cancel for antiparallel orientation, yielding a low and high superconducting transition temperature, respectively [126]. However, this cancellation is only complete if the thickness of the S layer is very small compared to $\xi_0(T_{c0})$, because this is the scale on which the induced exchange field decays into the S material, as discussed above.

In the F material of S/F bilayers and F/S/F trilayers, a spatial modulation of the singlet mixed with the spin-projection zero triplet pairing amplitude occurs [128]. The critical temperature depends on the pairing wave function flux through the boundary between the S and F layer(s). For finite F layers, the modulation of the pairing amplitude yields interference phenomena depending on its phase at the outer interface of the F layer, thus, changing the pairing amplitude flux and modulating T_c as a function of the interference condition and, thus, as a function of d_F [9,10,129]. In a F/S/F trilayer, the boundary conditions at the two S/F interfaces are different for parallel and antiparallel configuration of the magnetizations (see the Appendix of Ref. [9]), resulting in a superconducting transition temperature, which depends on the relative orientation of the magnetizations. For antiparallel configurations the T_c can both be higher or lower than for the parallel configuration, which corresponds to a standard [15,20] or inverse spin-valve effect [20], respectively.

APPENDIX B: SATURATION MAGNETIC MOMENTS/MAGNETIZATIONS

1. Sample of the present work for decreasing magnetic field

In this section, the superscript *dec* to indicate decreasing field has been dropped for the sake of clarity of the formulas.

The saturation magnetic moments, m_S, for the major and the minor magnetic transition at decreasing field are obtained at $H_S = 50$ kOe from a fit of $\frac{\partial m}{\partial H_D}$ in the range from $H_D = -2.0$ to -4.5 kOe, using

$$\frac{\partial m}{\partial H_D} = \frac{2}{\pi}\left[\frac{m_{s,\mathrm{maj}}\, H_{t,\mathrm{maj}}}{H_{t,\mathrm{maj}}^2 + (H_D - H_{c,\mathrm{maj}})^2} + \frac{m_{s,\mathrm{min}}\, H_{t,\mathrm{min}}}{H_{t,\mathrm{min}}^2 + (H_D - H_{c,\mathrm{min}})^2}\right] + s \qquad \text{(B1)}$$

with H_t a threshold field (determining the field relative to the coercive field, at which half of the saturation magnetization is realized) and H_c the coercive field of the respective layers and s a constant offset due to dia-, para-, and antiferromagnetic contributions. This is the field derivative equivalent to the model by Geiler *et al.* [66]. Prior to the fit in Fig. 5(c), the offset has been evaluated from a fit of the high field data ($|H_D| = 25 - 50$ kOe) of the field derivative of the magnetization, where all ferromagnetic layers are saturated, yielding $s = -(6.924 \pm 0.008) \times 10^{-6}$ emu/kOe. Figure 5(c) shows the derivative, the fit according to Eq. (B1) and the individual contributions from both layers. The fit parameters obtained are given in Table I.

TABLE I. Fit parameters obtained by fitting Eq. (B1) for decreasing H_D [see Fig. 5(c)].

Fit Parameter	Value
$m_{s,\mathrm{maj}}$	$(1.13 \pm 0.02) \times 10^{-4}$ emu
$m_{s,\mathrm{min}}$	$(0.053 \pm 0.012) \times 10^{-4}$ emu
$H_{t,\mathrm{maj}}$	313 ± 7 Oe
$H_{t,\mathrm{min}}$	120 ± 32 Oe
$H_{c,\mathrm{maj}}$	-2.834 ± 0.004 kOe
$H_{c,\mathrm{min}}$	-3.587 ± 0.022 kOe

Assigning the major and minor transition to the Co and bottom $Cu_{41}Ni_{59}$ layer, respectively, we can calculate the magnetic moment per atom from the saturation magnetic moment according to

$$\frac{m_{at}}{\mu_B} = \frac{m_S \,/\left(N_A \frac{V_L}{V_m}\right)}{0.9274 \times 10^{-20}\ \mathrm{emu}}. \qquad \text{(B2)}$$

Here, V_L, is the volume of the respective layer, V_m is the molar volume of the respective material, N_A the Avogadro constant, and $\mu_B = 0.9274 \times 10^{-20}$ emu [84] the Bohr magneton.

The molar volume can be obtained from the molar mass, M_m and and the density ρ, using $V_m = M_m/\rho$.

The density of fcc-Co has been calculated using the molar mass and knowledge of the unit cell according to

$$\rho_{\text{fcc-Co}} = \frac{M_m \frac{N_{fcc}}{N_A}}{a^3_{\text{fcc-Co}}} \qquad \text{(B3)}$$

with $a_{\text{fcc-Co}} = 3.548$ Å (obtained from x-ray powder diffraction, see p. 2062 of Ref. [130], and Ref. [131]) and the number of atoms in a fcc unit cell, $N_{fcc} = 4$.

The molar volume of the $Cu_{41}Ni_{59}$ alloy has been calculated according to Vegard's rule [132] by

$$V_{m,\mathrm{CuNi}} = 0.41 V_{m,\mathrm{Cu}} + 0.59 V_{m,\mathrm{Ni}} \qquad \text{(B4)}$$

using the V_m for Cu and Ni, as calculated from the corresponding literature values for M_m and ρ from [133] (see Table II). The density can be calculated analogously as linear interpolation between Cu and Ni.

All material parameters and results for Cu, Ni, $Cu_{41}Ni_{59}$, fcc-Co, and hcp-Co are summarized in Table II.

Using Eq. (B2) and V_L, calculated from the cross-sectional area, A, of the sample (10 mm × 2.3 mm = 23 mm^2) and the thickness, d, of the Co and the bottom $Cu_{41}Ni_{59}$ layer,

TABLE II. Material parameters for hcp-, fcc-Co, Cu, Ni, and $Cu_{41}Ni_{59}$. The values indicated by the asterisk are calculated according to the details in the text. The density of hcp Co has been taken from Ref. [134], all other parameters are taken from Ref. [133].

Parameter	hcp-Co	fcc-Co	Cu	Ni	$Cu_{41}Ni_{59}$
M_m [g/mol]	58.93	58.93	63.55	58.71	n/a
ρ[g/cm^3]	8.90	8.77*	8.96	8.90	8.92*
V_m[cm^3/mol]	6.62*	6.72*	7.09*	6.60*	6.80*

TABLE III. Layer properties for the $Cu_{41}Ni_{59}$ and the Co layer. If two values are given for the Co layer, they are calculated assuming a hcp and fcc structure, respectively.

Parameter	hcp/fcc Co	bottom $Cu_{41}Ni_{59}$
A[mm^2]	23	23
d [nm]	4.6	2.2
V_L[cm^3]	106×10^{-9}	51×10^{-9}
m_s[10^{-4} emu]	1.13 ± 0.02	0.053 ± 0.012
m_{at}[μ_B]	1.27 ± 0.02 / 1.29 ± 0.02	0.13 ± 0.03
M_s[emu/cm^3]	1070 ± 20	105 ± 24
$\tilde{M}_s$ [emu/g]	120 ± 2 / 122 ± 2	12 ± 3

respectively, and the molar volumes from Table II, we calculate the magnetic moment per atom. The relevant quantities and results are summarized in Table III. Here, also the saturation magnetization, $M_s = m_s/V_L$, i.e., the saturation magnetic moment per volume, and the specific saturation magnetization, $\tilde{M}_s = M_s/\rho$, i.e., the saturation magnetic moment per mass, are given.

The atomic magnetic moment obtained for the bottom $Cu_{41}Ni_{59}$ layer is close to the value for bulk material of 0.14 μ_B [135] and values of 0.14 μ_B and 0.16 μ_B, which we obtained from SQUID measurements on stand-alone $Cu_{41}Ni_{59}$ films in our former work [9]. Thus, the assignment of the minor transition for decreasing H_D to the bottom $Cu_{41}Ni_{59}$ layer, is considered reasonable.

In Table IV we collected various results for the magnetic moment, the magnetization, and the specific magnetization for different systems and structures. In Ref. [136], the flux density associated with the saturation magnetization is given to be $J_S = 1.82$ T. The related saturation magnetization is $M_S = J_S/\mu_0$ with $\mu_0 = 4\pi \times 10^{-7}$ Vs/(Am). To obtain the results in the cgs-emu system from the international SI system we use that 1 emu/cm^3 $\equiv$ 10^3 A/m [64]. Since $M_S = m_s/V_L$ we obtain m_{at} according to Eq. (B2). In Ref. [137] the value for $\tilde{M}_S$ is given in Fig. 5 on p. 190.

It is apparent from the data in Table IV, that the magnetization of hcp-Co tends to be higher than for fcc-Co. Since the magnetization obtained for the Co layer in the present work can even be classified as the lower end of the fcc results, we conclude, that our Co film has fcc structure. However, a definite classification as fcc-Co can only be obtained by structural analysis.

2. Sample of the present work for increasing magnetic field

Due to the lack of clear structures in $\partial m/\partial H_D$ for increasing H_D, a direct fit by Eq. (B1) is not possible. Maybe even the shape of the peak does not satisfy this model, as it appears to be asymmetric with respect to the field. Nevertheless, a rough estimation of the magnetic moment of the major transition yields $m_{S,\mathrm{major}} = 1.1 \times 10^{-4}$ emu (superscript "inc" omitted), which is close to the one obtained for the Co layer in decreasing field. For the minor transition, no reliable estimation could be obtained.

APPENDIX C: CONSIDERATIONS OF VARYING EXCHANGE COUPLING

Taking into account a varying exchange coupling, which is strongly depending on the anisotropies in the ferromagnetic and antiferromagnetic layers, due to different local compositions and even different local magnetic anisotropies of CoO_x [80,97], we will discuss possible origins and results of such variations in the following.

The compositions of CoO_x strongly affects the Néel temperature, T_N. This can lead to different sequences of magnetic ordering when field cooling. The Néel temperature of CoO films is higher than the Curie temperature, Θ_C expected for our $Cu_{41}Ni_{59}$ films (although T_N possibly reduced below the bulk material value of about 290 K [140,141], as discussed in Refs. [142–145], it is close to the bulk value even for a film thickness of 10 nm). We observed $\Theta_C \approx$ 110–120 K for stand-alone $Cu_{41}Ni_{59}$ films in Ref. [9], close to the results of Refs. [146] and [147]. This is below the bulk material value of 180 K [135]. Because the thickness of the $Cu_{41}Ni_{59}$ layers in the present work is smaller than in Ref. [9], a further reduction of Θ_C is expected [68]. For Co_3O_4 the relative temperatures are vice versa, even without considering a reduction of the Néel temperatures [148–151] below the bulk value of about 40 K [150,152,153]. These different relative ordering temperatures affect the appearance of exchange bias in the system [97].

It has been observed in Ni/Co_3O_4 thin film bilayers [154], that very thin CoO and NiO layers are formed by a solid-state reaction at the interface, yielding exchange bias to persist up to

TABLE IV. Literature values for the magnetic moment, the magnetization, and the specific magnetization for different systems and structures. Values indicate by the asterisk are calculated from the literature values using Table II.

Structure	System	Thickness (nm)	m_{at} (μ_b)	M_s (emu/cm^3)	$\tilde{M}_s$ (emu/g)	Reference
hcp	Bulk $H \parallel c$ axis	n/a	1.729	1460*	164*	[138]
hcp	Bulk $H \perp c$ axis	n/a	1.721	1450*	163*	[138]
hcp	Films on W substrate	0.5–10	1.72*	1450	163*	[136]
hcp	MBE-grown Co-Au superlattices	0.5–4	1.50–1.65*	1267–1393	142–156*	[75]
fcc	Bulk	n/a	1.56*	1300*	147.9	[137]
fcc	Bulk	n/a	1.69*	1400	160*	[139]
fcc	Evaporated films between thin Cu layers	1–10	1.36*	1131	129*	[139]
fcc	Sputtered films between thin Cu layers	1–10	1.60*	1333	152*	[139]
fcc	MBE-grown Co-Cu superlattices	0.5–4	1.40–1.57*	1160–1302	132–148*	[75]

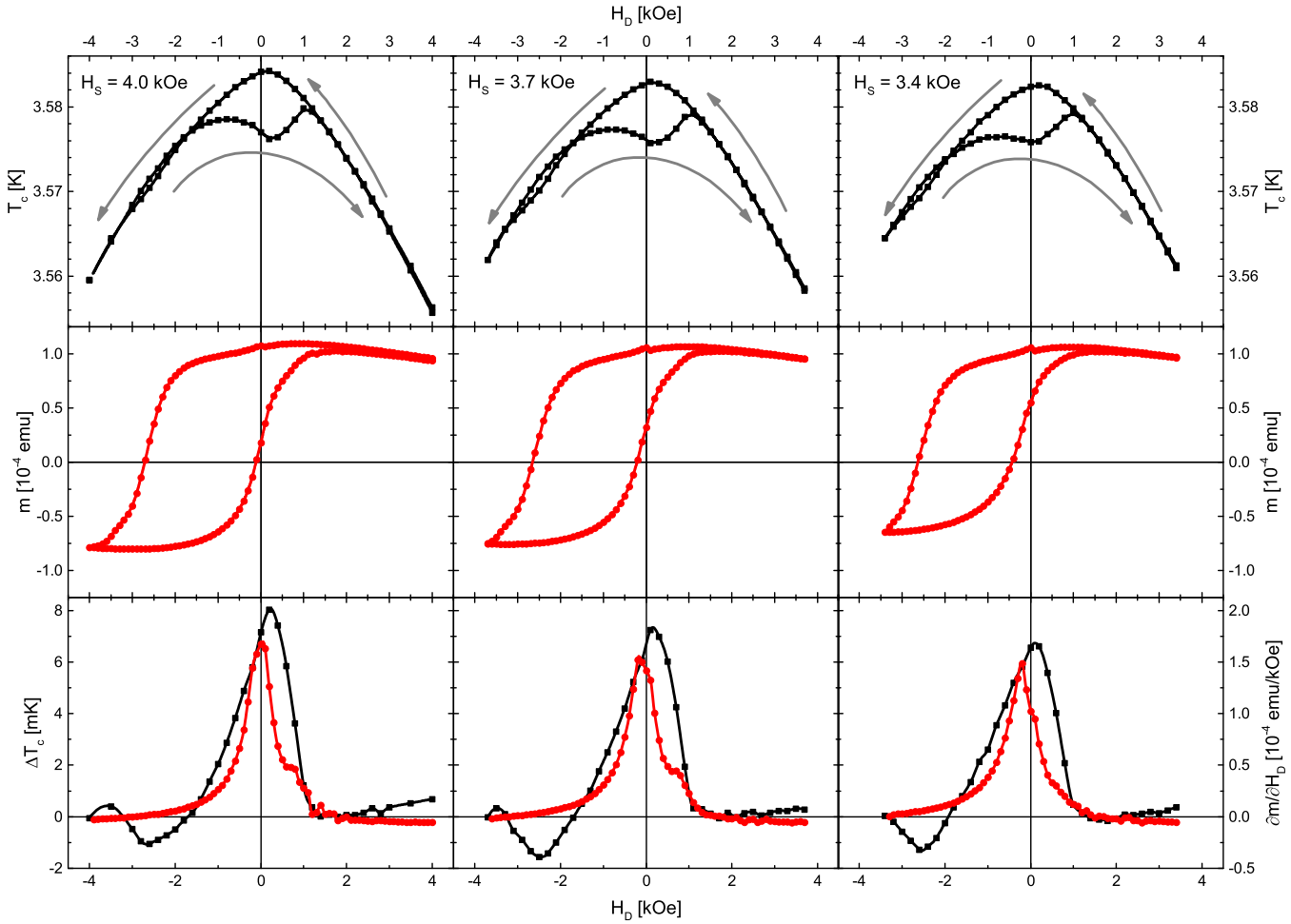

FIG. 11. Selected data obtained for different magnetic field sweep widths, H_S. Top: Superconducting transition temperature, $T_c(H_D)$, for increasing and decreasing applied field, H_D. The arrows indicate the sweep direction. Middle: Magnetic moment hysteresis loop, $m(H_D)$. Bottom: SSV effect, $\Delta T_c(H_D)$ (black squares) and field derivative of the magnetic hysteresis loop for decreasing field, $\partial m/\partial H_D$ (red dots). In all panels, the solid lines are guide to the eye.

temperatures far above the T_N of bulk Co_3O_4. In this system, the antiferromagnetic NiO layer can mediate the exchange bias between the CoO and the Ni films. A similar effect is possible to occur in the sample of the present work between the bottom $Cu_{41}Ni_{59}$ layer and possible Co_3O_4 grains, tending to even out the different exchange bias strength for different local compositions.

Even if different exchange bias strengths are present, the exchange interaction within the bottom $Cu_{41}Ni_{59}$ will tend to smear out these differences. The shortest scale on which nonhomogeneous magnetization can exist in a ferromagnetic material is given by the exchange stiffness length, l_{ex}.

In Eqs. (7.8) of his book [84], Coey gives an expression for l_{ex}. Using the expression he gives for the exchange stiffness (Eq. (7.7) of Ref. [84]) and the relation of the Curie temperature and the exchange constant (Eq. (5.26) of Ref. [84]), we obtain

$$l_{ex} = \sqrt{\frac{A}{\mu_0 M_S^2}}, \quad \text{with} \quad A = \frac{3k_B\Theta_c}{2a_m} \times \frac{Z_c}{Z}. \tag{C1}$$

Here, A is the exchange stiffness, Z_c the number of magnetic atoms per unit cell, Z the number of magnetic nearest neighbors, a_m the lattice constant of the magnetic unit cell (for elemental magnets this is equal to the materials lattice constant a_0), and k_B Boltzmann's constant.

For the bottom $Cu_{41}Ni_{59}$ layer of the present work, it is $M_S = 105\ \text{emu/cm}^3 \equiv 105 \times 10^3\ \text{A/m}$ (converted to SI units [64]). A typical value, we obtained for stand-alone $Cu_{41}Ni_{59}$ film is $\Theta_c = 115$ K (see above). For our diluted magnetic alloy we assume that the ratio of $Z = 12$ and $Z_c = 4$ (for a fcc lattice) remains constant upon dilution. With $a_{0,\text{Cu}} = 3.597$ Å and $a_{0,\text{Ni}} = 3.499$ Å [155], we obtain $a_{0,\text{Cu41Ni59}} = 3.539$ Å, applying Vegard's rule [132]. Using $a_m = a_{0,\text{Cu41Ni59}}$, this results in $l_{ex} = 13$ nm for our bottom $Cu_{41}Ni_{59}$ layer.

For the Co/CoOx exchange coupling, T_N is well below Θ_C of the Co film. A strong reduction of Θ_C below the bulk value of 1390 K (see Table 33.1 of Ref. [156], Ref. [157]) is reported only for ultrathin films below six monolayers. The suppression is more pronounced for fcc-Co [73,74,158,159] than for hcp-Co [160].

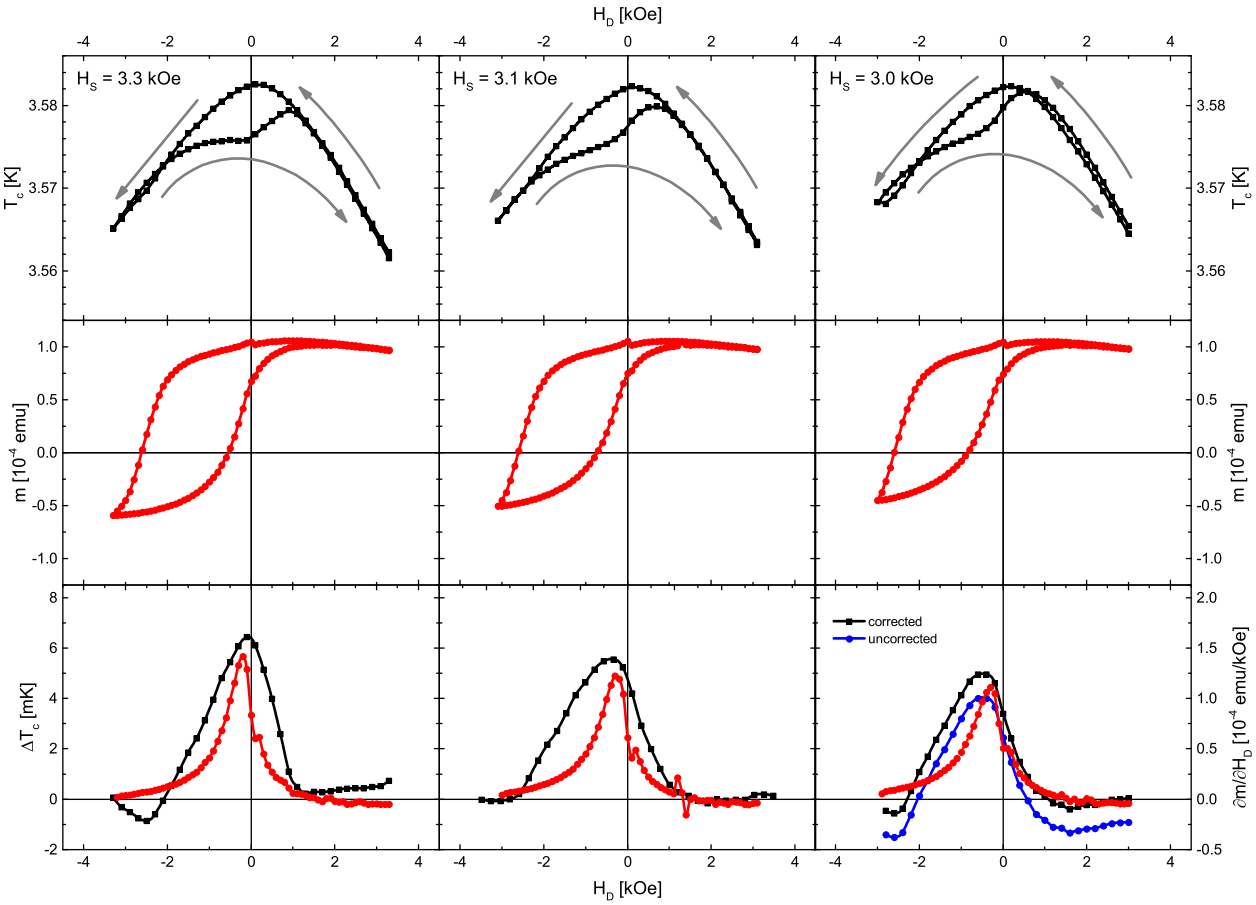

FIG. 12. Selected data obtained for different magnetic field sweep widths, H_S. Top: Superconducting transition temperature, $T_c(H_D)$, for increasing and decreasing applied field, H_D. The arrows indicate the sweep direction. Middle: Magnetic moment hysteresis loop, $m(H_D)$. Bottom: SSV effect, $\Delta T_c(H_D)$ (black squares) and field derivative of the magnetic hysteresis loop, $\partial m/\partial H_D$ (red dots). In all panels, the solid lines are guide to the eye. For a discussion of the correction of ΔT_c in the bottom right panel see the text.

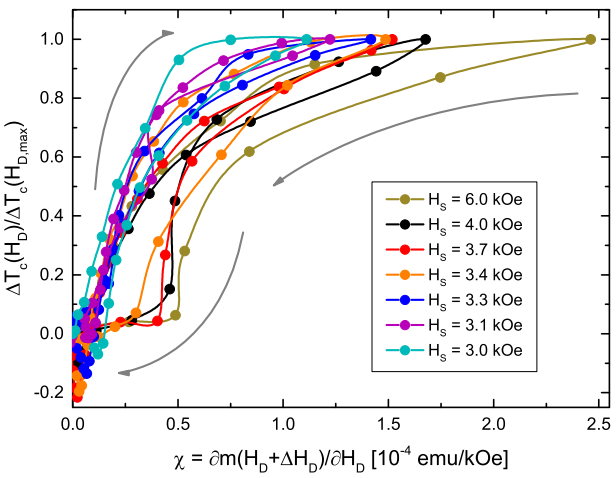

FIG. 13. Superconducting spin-valve effect, $\Delta T_c(H_D)$, normalized to the maximum value $\Delta T_c(H_{D,\max})$ for the respective H_S, as a function of the field derivative $\chi = \frac{\partial m(H_D+\Delta H_D)}{\partial H_D}$ for increasing H_D. Here, ΔH_D is the field shift between the maximum of the derivative and the maximum of the effect. The arrows indicate the sequence of data points from negative H_D to positive H_D (starting at zero χ). Solid lines are guide to the eye.

APPENDIX D: SSV EFFECT ΔT_c IN COMPARISON WITH $m(H_D)$ AND $\partial m/\partial H_D$

In Figs. 11 and 12, a series of figures are shown, which demonstrate the relation between the $T_c(H_D)$ data, the magnetic hysteresis curve, $m(H_D)$, and its field derivative for different sweep widths, H_S. In the T_c data of Fig. 12 right column (blue symbols/line), an apparent offset between the leftward and rightward sweep, nonvanishing even for the region of magnetic saturation at the positive reversal, has been observed. Thus, we corrected for this offset (see black symbols/line) to obtain data points for the correlation with the magnetic data in Figs. 8 and 13.

APPENDIX E: SSV EFFECT VS FIELD DERIVATIVE OF MAGNETIC MOMENT HYSTERESIS DATA FOR INCREASING FIELD

In Fig. 13 the SSV effect at H_D is plotted as a function of the field derivative, $\chi = \partial m(H_D + \Delta H_D)/\partial H_D$, for different sweep width, H_S. This is essentially the same plot as Fig. 8, however, the different sweep widths are indicated by coloring.

[1] P. Fulde and R. Ferrell, Phys. Rev. **135**, A550 (1964).
[2] A. I. Larkin and Y. N. Ovchinnikov, Sov. Phys. JETP **20**, 762 (1965).
[3] G. Zwicknagl and J. Wosnitza, Int. J. Mod. Phys. B **24**, 3915 (2010).
[4] J. Bardeen, L. N. Cooper, and J. R. Schrieffer, Phys. Rev. **108**, 1175 (1957).
[5] L. R. Tagirov, Physica C (Amsterdam) **307**, 145 (1998).
[6] A. I. Buzdin, Rev. Mod. Phys. **77**, 935 (2005).
[7] M. Eschrig, Phys. Today **64**, 43 (2011).
[8] V. Zdravkov, A. Sidorenko, G. Obermeier, S. Gsell, M. Schreck, C. Müller, S. Horn, R. Tidecks, and L. R. Tagirov, Phys. Rev. Lett. **97**, 057004 (2006).
[9] V. I. Zdravkov, J. Kehrle, G. Obermeier, S. Gsell, M. Schreck, C. Müller, H.-A. Krug von Nidda, J. Lindner, J. Moosburger-Will, E. Nold, R. Morari, V. V. Ryazanov, A. S. Sidorenko, S. Horn, R. Tidecks, and L. R. Tagirov, Phys. Rev. B **82**, 054517 (2010).
[10] J. Kehrle, V. I. Zdravkov, G. Obermeier, J. Garcia-Garcia, A. Ullrich, C. Müller, R. Morari, A. S. Sidorenko, S. Horn, L. R. Tagirov, and R. Tidecks, Ann. Phys. (N.Y.) **524**, 37 (2011).
[11] M. N. Baibich, J. M. Broto, A. Fert, F. Nguyen Van Dau, F. Petroff, P. Etienne, G. Creuzet, A. Friederich, and J. Chazelas, Phys. Rev. Lett. **61**, 2472 (1988).
[12] G. Binasch, P. Grünberg, F. Saurenbach, and W. Zinn, Phys. Rev. B **39**, 4828 (1989).
[13] B. Dieny, V. S. Speriosu, S. Metin, S. S. P. Parkin, B. A. Gurney, P. Baumgart, and D. R. Wilhoit, J. Appl. Phys. **69**, 4774 (1991).
[14] S. Oh, D. Youm, and M. R. Beasley, Appl. Phys. Lett. **71**, 2376 (1997).
[15] L. R. Tagirov, Phys. Rev. Lett. **83**, 2058 (1999).
[16] A. I. Buzdin, A. V. Vedyayev, and N. V. Ryzhanova, Europhys. Lett. **48**, 686 (1999).
[17] C.-Y. You, Y. B. Bazaliy, J. Y. Gu, S. J. Oh, L. M. Litvak, and S. D. Bader, Phys. Rev. B **70**, 014505 (2004).
[18] Y. V. Fominov, A. A. Golubov, and M. Y. Kupriyanov, JETP Lett. **77**, 510 (2003).
[19] Y. V. Fominov, A. A. Golubov, T. Y. Karminskaya, M. Y. Kupriyanov, R. G. Deminov, and L. R. Tagirov, JETP Lett. **91**, 308 (2010).
[20] S. V. Mironov and A. I. Buzdin, Phys. Rev. B **89**, 144505 (2014).
[21] R. R. Gaifullin, R. G. Deminov, L. R. Tagirov, T. Y. Karminskaya, M. Y. Kupriyanov, and A. A. Golubov, J. Phys.: Conf. Ser. **690**, 012033 (2016).
[22] J. Y. Gu, C.-Y. You, J. S. Jiang, J. Pearson, Y. B. Bazaliy, and S. D. Bader, Phys. Rev. Lett. **89**, 267001 (2002).
[23] A. Potenza and C. H. Marrows, Phys. Rev. B **71**, 180503 (2005); **72**, 069901(E) (2005).
[24] J. Y. Gu, Y. B. Bazaliy, S. D. Bader, and C. Y. You, *Ferromagnetic-Superconducting Hybrid Systems, in The Theory of Quantum Transport in Metallic and Hybrid Nanostructures*, NATO Science Series II: Mathematics, Physics and Chemistry, Vol. 230, pp. 159–171, edited by A. Glatz, V. I. Kozub, and V. M. Vinokur (Springer, Dordrecht, 2006).
[25] I. C. Moraru, W. P. Pratt, and N. O. Birge, Phys. Rev. Lett. **96**, 037004 (2006).
[26] I. C. Moraru, W. P. Pratt, and N. O. Birge, Phys. Rev. B **74**, 220507 (2006).
[27] A. Y. Rusanov, S. Habraken, and J. Aarts, Phys. Rev. B **73**, 060505 (2006).
[28] J. Aarts and A. Y. Rusanov, C. R. Phys. **7**, 99 (2006).
[29] R. Steiner and P. Ziemann, Phys. Rev. B **74**, 094504 (2006).
[30] D. Stamopoulos, E. Manios, and M. Pissas, Phys. Rev. B **75**, 014501 (2007).
[31] A. Singh, C. Sürgers, and H. v. Löhneysen, Phys. Rev. B **75**, 024513 (2007).
[32] A. Singh, C. Sürgers, R. Hoffmann, H. v. Löhneysen, T. V. Ashworth, N. Pilet, and H. J. Hug, Appl. Phys. Lett. **91**, 152504 (2007).
[33] Dong Ho Kim and T. J. Hwang, Physica C (Amsterdam) **455**, 58 (2007).
[34] G. Nowak, H. Zabel, K. Westerholt, I. Garifullin, M. Marcellini, A. Liebig, and B. Hjörvarsson, Phys. Rev. B **78**, 134520 (2008).
[35] P. Cadden-Zimansky, Y. B. Bazaliy, L. M. Litvak, J. S. Jiang, J. Pearson, J. Y. Gu, C.-Y. You, M. R. Beasley, and S. D. Bader, Phys. Rev. B **77**, 184501 (2008).
[36] P. V. Leksin, R. I. Salikhov, I. R. Garifullin, H. Vinzelberg, V. Kataev, R. Klingeler, L. R. Tagirov, and B. Büchner, JETP Lett. **90**, 59 (2009).
[37] J. Zhu, X. Cheng, C. Boone, and I. N. Krivorotov, Phys. Rev. Lett. **103**, 027004 (2009).
[38] J. Zhu, I. N. Krivorotov, K. Halterman, and O. T. Valls, Phys. Rev. Lett. **105**, 207002 (2010).
[39] Y. Luo and K. Samwer, Europhys. Lett. **91**, 37003 (2010).
[40] Y. Gu, G. B. Halasz, J. W. A. Robinson, and M. G. Blamire, Phys. Rev. Lett. **115**, 067201 (2015).
[41] P. V. Leksin, N. N. Garif'yanov, I. A. Garifullin, J. Schumann, H. Vinzelberg, V. Kataev, R. Klingeler, O. G. Schmidt, and B. Büchner, Appl. Phys. Lett. **97**, 102505 (2010).
[42] P. V. Leksin, N. N. Garif'yanov, I. A. Garifullin, J. Schumann, V. Kataev, O. G. Schmidt, and B. Büchner, Phys. Rev. Lett. **106**, 067005 (2011).
[43] P. V. Leksin, N. N. Garif'yanov, I. A. Garifullin, J. Schumann, V. Kataev, O. G. Schmidt, and B. Büchner, Phys. Rev. B **85**, 024502 (2012).
[44] G. Nowak, K. Westerholt, and H. Zabel, Supercond. Sci. Technol. **26**, 025004 (2013).
[45] P. V. Leksin, A. A. Kamashev, N. N. Garif'yanov, I. A. Garifullin, Y. V. Fominov, J. Schumann, C. Hess, V. Kataev, and B. Büchner, JETP Lett. **97**, 478 (2013).
[46] C.-T. Wu, O. T. Valls, and K. Halterman, Phys. Rev. B **86**, 014523 (2012).
[47] V. I. Zdravkov, J. Kehrle, G. Obermeier, D. Lenk, H.-A. Krug von Nidda, C. Müller, M. Y. Kupriyanov, A. S. Sidorenko, S. Horn, R. Tidecks, and L. R. Tagirov, Phys. Rev. B **87**, 144507 (2013).
[48] P. V. Leksin, N. N. Garif'yanov, I. A. Garifullin, Y. V. Fominov, J. Schumann, Y. Krupskaya, V. Kataev, O. G. Schmidt, and B. Büchner, Phys. Rev. Lett. **109**, 057005 (2012).
[49] X. L. Wang, A. Di Bernardo, N. Banerjee, A. Wells, F. S. Bergeret, M. G. Blamire, and J. W. A. Robinson, Phys. Rev. B **89**, 140508(R) (2014).
[50] A. A. Jara, C. Safranski, I. N. Krivorotov, C. T. Wu, A. N. Malmi-Kakkada, O. T. Valls, and K. Halterman, Phys. Rev. B **89**, 184502 (2014).
[51] A. Singh, S. Voltan, K. Lahabi, and J. Aarts, Phys. Rev. X **5**, 021019 (2015).

[52] M. G. Flokstra, T. C. Cunningham, J. Kim, N. Satchell, G. Burnell, P. J. Curran, S. J. Bending, C. J. Kinane, J. F. K. Cooper, S. Langridge, A. Isidori, N. Pugach, M. Eschrig, and S. L. Lee, Phys. Rev. B **91**, 060501(R) (2015).

[53] P. V. Leksin, N. N. Garif'yanov, A. A. Kamashev, Y. V. Fominov, J. Schumann, C. Hess, V. Kataev, B. Büchner, and I. A. Garifullin, Phys. Rev. B **91**, 214508 (2015).

[54] D. Lenk, V. I. Zdravkov, J.-M. Kehrle, G. Obermeier, A. Ullrich, R. Morari, H.-A. Krug von Nidda, C. Müller, M. Y. Kupriyanov, A. S. Sidorenko, S. Horn, R. G. Deminov, L. R. Tagirov, and R. Tidecks, Beilstein J. Nanotechnol. **7**, 957 (2016).

[55] P. V. Leksin, N. N. Garif'yanov, A. A. Kamashev, A. A. Validov, Y. V. Fominov, J. Schumann, V. Kataev, J. Thomas, B. Büchner, and I. A. Garifullin, Phys. Rev. B **93**, 100502(R) (2016).

[56] N. Banerjee, C. B. Smiet, R. G. J. Smits, A. Ozaeta, F. S. Bergeret, M. G. Blamiere, and J. W. A. Robinson, Nature Commun. **5**, 3048 (2014).

[57] V. I. Zdravkov, D. Lenk, R. Morari, A. Ullrich, G. Obermeier, C. Müller, H.-A. Krug von Nidda, A. S. Sidorenko, S. Horn, R. Tidecks, and L. R. Tagirov, Appl. Phys. Lett. **103**, 062604 (2013).

[58] F. Radu and H. Zabel, *Exchange Bias Effect of Ferro/Antiferromagnetic Heterostructures, in Magnetic Heterostructures*, Chap. 3, STMP Vol. 227, edited by H. Zabel and S. D. Bader (Springer, Berlin, 2008).

[59] J. W. A. Robinson, Physics **8**, 49 (2015).

[60] J. Slaughter, M. DeHerrera, and H. Dürr, *Magnetoresistive RAM*, Nanoelectronics and Information Technology, Chap. 23, edited by R. Waser (Wiley-VCH, Weinheim, 2003).

[61] J. Linder and J. W. A. Robinson, Nature Phys. **11**, 307 (2015).

[62] G.-X. Miao, A. V. Ramos, and J. S. Moodera, Phys. Rev. Lett. **101**, 137001 (2008).

[63] B. Li, N. Roschewsky, B. A. Assuf, M. Eich, M. Epstein-Martin, D. Heiman, M. Münzenberg, and J. S. Moodera, Phys. Rev. Lett. **110**, 097001 (2013).

[64] R. B. Goldfarb and F. R. Fickett, *Units for Magnetic Properties*, NBS Special Publication No. 696 (National Bureau of Standards, Boulder, 1985).

[65] S. Brems, D. Buntinx, K. Temst, C. Van Haesendonck, F. Radu, and H. Zabel, Phys. Rev. Lett. **95**, 157202 (2005).

[66] A. L. Geiler, V. G. Harris, V. Vittoria, and N. X. Sun, J. Appl. Phys. **99**, 08B316 (2006).

[67] A. S. Sidorenko, D. Lenk, V. I. Zdravkov, R. Morari, A. Ullrich, C. Müller, H. A. Krug von Nidda, S. Horn, L. R. Tagirov, and R. Tidecks, *Cobalt/Cobaltoxide Exchange Bias System for Diluted Ferromagnetic Alloy Films in Superconducting Spin-Valves*, Nanostructures and Thin Films for Multifunctional Applications - Technology, Properties and Devices, Series NanoScience, Technology, edited by I. Tiginyanu, P. Topalu, and V. Ursaki, Chap. 9, p. 301 (Springer International Publishing, Cham, 2016). There is a typo in Ref. 62 of this work, the page number should read 144507.

[68] A. Ruotolo, C. Bell, C. W. Leung, and M. G. Blamire, J. Appl. Phys. **96**, 512 (2004).

[69] I. S. Veshchunov, V. A. Oboznov, A. N. Rossolenko, A. S. Prokofiev, L. Y. Vinnikov, A. Y. Rusanov, and D. V. Matveev, JETP Lett. **88**, 758 (2008).

[70] J.-M. Kehrle, Ph.D. thesis, Universität Augsburg, 2012.

[71] C. Chappert, K. Le Dang, P. Beauvillain, H. Hurdequint, and D. Renard, Phys. Rev. B **34**, 3192 (1986).

[72] C. Chappert and P. Bruno, J. Appl. Phys. **64**, 5736 (1988).

[73] C. M. Schneider, P. Bressler, P. Schuster, J. Kirschner, J. J. de Miguel, R. Miranda, and S. Ferrer, Vacuum **41**, 503 (1990).

[74] C. M. Schneider, P. Bressler, P. Schuster, J. Kirschner, J. J. de Miguel, and R. Miranda, Phys. Rev. Lett. **64**, 1059 (1990).

[75] C. H. Lee, H. He, F. J. Lamelas, W. Vavra, C. Uher, and R. Clarke, Phys. Rev. B **42**, 1066 (1990).

[76] M. Gierlings, M. J. Prandolini, H. Fritzsche, M. Gruyters, and D. Riegel, Phys. Rev. B **65**, 092407 (2002).

[77] F. Radu, M. Etzkorn, R. Siebrecht, T. Schmitte, K. Westerholt, and H. Zabel, Phys. Rev. B **67**, 134409 (2003).

[78] W.-T. Lee, S. G. E. te Velthuis, G. P. Felcher, F. Klose, T. Gredig, and E. D. Dahlberg, Phys. Rev. B **65**, 224417 (2002).

[79] U. Welp, S. G. E. te Velthuis, G. P. Felcher, T. Gredig, and E. D. Dahlberg, J. Appl. Phys. **93**, 7726 (2003).

[80] U. Nowak, K. D. Usadel, J. Keller, P. Miltényi, B. Beschoten, and G. Güntherodt, Phys. Rev. B **66**, 014430 (2002).

[81] J. Keller, P. Miltényi, B. Beschoten, G. Güntherodt, U. Nowak, and K. D. Usadel, Phys. Rev. B **66**, 014431 (2002).

[82] A. Scholl, M. Liberati, E. Arenholz, H. Ohldag, and J. Stöhr, Phys. Rev. Lett. **92**, 247201 (2004).

[83] E. E. Fullerton, J. S. Jiang, and S. D. Bader, J. Magn. Magn. Mater. **200**, 392 (1999).

[84] J. M. D. Coey, *Magnetism and Magnetic Materials* (Cambridge University Press, Cambridge, 2010).

[85] F. S. Bergeret, A. F. Volkov, and K. B. Efetov, Rev. Mod. Phys. **77**, 1321 (2005).

[86] I. Sosnin, H. Cho, V. T. Petrashov, and A. F. Volkov, Phys. Rev. Lett. **96**, 157002 (2006).

[87] J. Y. Gu, J. Kusnadi, and C.-Y. You, Phys. Rev. B **81**, 214435 (2010).

[88] L. Y. Zhu, Y. Liu, F. S. Bergeret, J. E. Pearson, S. G. E. te Velthuis, S. D. Bader, and J. S. Jiang, Phys. Rev. Lett. **110**, 177001 (2013).

[89] T. Champel and M. Eschrig, Phys. Rev. B **72**, 054523 (2005).

[90] T. Champel and M. Eschrig, Phys. Rev. B **71**, 220506 (2005).

[91] P. Grünberg, R. Schreiber, Y. Pang, M. B. Brodsky, and H. Sowers, Phys. Rev. Lett. **57**, 2442 (1986).

[92] S. S. P. Parkin, N. More, and K. P. Roche, Phys. Rev. Lett. **64**, 2304 (1990).

[93] P. Grünberg, S. Demokritov, A. Fuss, M. Vohl, and J. A. Wolf, J. Appl. Phys. **69**, 4789 (1991).

[94] A. Azevedo, C. Chesman, S. M. Rezende, F. M. de Aguiar, X. Bian, and S. S. P. Parkin, Phys. Rev. Lett. **76**, 4837 (1996).

[95] S. O. Demokritov, J. Phys. D: Appl. Phys. **31**, 925 (1998).

[96] J. Camarero, Y. Pennec, J. Vogel, M. Bonfim, S. PizziNi, F. Ernult, F. Fettar, F. Garcia, F. Lançon, L. Billard, B. Dieny, A. Tagliaferri, and N. B. Brookes, Phys. Rev. Lett. **91**, 027201 (2003).

[97] M. G. Blamire, M. Ali, C.-W. Leung, C. H. Marrows, and B. J. Hickey, Phys. Rev. Lett. **98**, 217202 (2007).

[98] M. Flokstra and J. Aarts, Phys. Rev. B **80**, 144513 (2009).

[99] D. Lenk, M. Hemmida, R. Morari, V. I. Zdravkov, A. Ullrich, C. Müller, A. S. Sidorenko, S. Horn, L. R. Tagirov, A. Loidl, H.-A. Krug von Nidda, and R. Tidecks, Phys. Rev. B **93**, 184501 (2016).

[100] Y. Cao, K. Xu, W. Jiang, T. Droubay, P. Ramuhalli, D. Edwards, B. R. Johnson, and J. McCloy, J. Magn. Magn. Mater. **395**, 361 (2015).

[101] T. J. Hwang and Dong Ho. Kim, Appl. Phys. Lett. **101**, 072601 (2012).

[102] S. G. Doettinger, R. P. Huebener, R. Gerdemann, A. Kühle, S. Anders, T. G. Träuble, and J. C. Villégier, Phys. Rev. Lett. **73**, 1691 (1994).

[103] E. A. Ilyina, C. Cirillo, and C. Attanasio, Eur. Phys. J. B **83**, 53 (2011).

[104] C. Attanasio and C. Cirillo, J. Phys.: Condens. Matter **24**, 083201 (2012).

[105] W. J. Skocpol, M. R. Beasley, and M. Tinkham, J. Appl. Phys. **45**, 4054 (1974).

[106] H. J. Schulze and K. Keck, Z. Phys. B **51**, 215 (1983).

[107] H. J. Schulze and K. Keck, Appl. Phys. A **34**, 243 (1984).

[108] A. V. Gurevich and R. G. Mints, Rev. Mod. Phys. **59**, 941 (1987).

[109] G. Sarma, J. Phys. Chem. Solids. **24**, 1029 (1963).

[110] P. G. de Gennes, Phys. Lett. **23**, 10 (1966).

[111] G. Deutscher and F. Meunier, Phys. Rev. Lett. **22**, 395 (1969).

[112] J. J. Hauser, Phys. Rev. Lett. **23**, 374 (1969).

[113] M. L. Kulic and M. Endres, Phys. Rev. B **62**, 11846 (2000).

[114] P. M. Tedrow, J. E. Tkaczyk, and A. Kumar, Phys. Rev. Lett. **56**, 1746 (1986).

[115] J. E. Tkaczyk and P. M. Tedrow, J. Appl. Phys. **61**, 3368 (1987).

[116] J. S. Moodera, X. Hao, G. A. Gibson, and R. Meservey, Phys. Rev. Lett. **61**, 637 (1988).

[117] X. Hao, J. S. Moodera, and R. Meservey, Phys. Rev. B **42**, 8235 (1990).

[118] X. Hao, J. S. Moodera, and R. Meservey, Phys. Rev. Lett. **67**, 1342 (1991).

[119] R. Meservey and P. M. Tedrow, Phys. Rep. **238**, 173 (1994).

[120] Y. M. Xiong, S. Stadler, P. W. Adams, and G. Catelani, Phys. Rev. Lett. **106**, 247001 (2011).

[121] M. J. Wolf, C. Sürgers, G. Fischer, and D. Beckmann, Phys. Rev. B **90**, 144509 (2014).

[122] R. Meservey, P. M. Tedrow, and P. Fulde, Phys. Rev. Lett. **25**, 1270 (1970).

[123] P. M. Tedrow and R. Meservey, Phys. Rev. Lett. **26**, 192 (1971).

[124] P. M. Tedrow and R. Meservey, Phys. Rev. Lett. **27**, 919 (1971).

[125] P. Fulde, Adv. Phys. **22**, 667 (1973).

[126] T. Tokuyasu, J. A. Sauls, and D. Rainer, Phys. Rev. B **38**, 8823 (1988).

[127] R. Tidecks, *Current Induced Nonequilibrium Phenomena in Quasi-One-Dimensional Superconductors, Chap. 5.1*, Springer Tracts in Modern Physics, Vol. 121 (Springer-Verlag, Berlin, 1990).

[128] M. Eschrig, Rep. Prog. Phys. **78**, 104501 (2015).

[129] A. S. Sidorenko, V. I. Zdravkov, J. Kehrle, R. Morari, E. Antropov, G. Obermeier, S. Gsell, M. Schreck, C. Müller, V. V. Ryazanov, S. Horn, R. Tidecks, and L. R. Tagirov, *Extinction and Recovery of Superconductivity by Interference in Superconductor/Ferromagnet Bilayers*, Nanoscale Phenomena — Fundamentals and Applications, Chap. 1, edited by H. Hahn, A. Sidorenko, and I. Tiginyanu (Springer-Verlag, Berlin, 2009).

[130] J. R. Cerdá, P. L. de Andres, A. Cebollada, R. Miranda, E. Navas, P. Schuster, C. M. Schneider, and J. Kirschner, J. Phys.: Condens. Matter **5**, 2055 (1993).

[131] E. A. Owen and D. M. Jones, Proc. Phys. Soc. B **67**, 456 (1954).

[132] A. R. Denton and N. W. Ashcroft, Phys. Rev. A **43**, 3161 (1991).

[133] R. C. West, *Handbook of Chemistry and Physics*, 56th ed., pp. B1–B42 (CRC Press, Cleveland, 1975).

[134] H. Keure, *Taschenlexikon der Chemie* (VEB Deutscher Verlag für Grundstoffindustrie, Leipzig, 1999).

[135] S. A. Ahern, M. J. C. Martin, and W. Sucksmith, Proc. R. Soc. London A **248**, 145 (1958).

[136] H. Fritzsche, J. Kohlhepp, and U. Gradmann, Phys. Rev. B **51**, 15933 (1995).

[137] Q. Meng, S. Guo, X. Zhao, and S. Veintemillas-Verdaguer, J. Alloy Compounds **580**, 187 (2013).

[138] R. Pauthenet, J. Appl. Phys. **53**, 8187 (1982).

[139] J. M. Beaujour, W. Chen, D. Kent, and J. Z. Sun, J. Appl. Phys. **99**, 08N503 (2006).

[140] W. L. Roth, Phys. Rev. **110**, 1333 (1958).

[141] W. Jauch, M. Reehuis, H. J. Bleif, F. Kubanek, and R. Pattison, Phys. Rev. B **64**, 052102 (2001).

[142] E. N. Abarra, K. Takano, F. Hellman, and A. E. Berkowitz, Phys. Rev. Lett. **77**, 3451 (1996).

[143] T. Ambrose and C. L. Chien, Phys. Rev. Lett. **76**, 1743 (1996).

[144] Y. J. Tang, D. J. Smith, B. L. Zink, F. Hellman, and A. E. Berkowitz, Phys. Rev. B **67**, 054408 (2003).

[145] M. Molina-Ruiz, A. F. Lopeandia, F. Pi, D. Givord, O. Bourgeois, and J. Rodriguez-Viejo, Phys. Rev. B **83**, 140407 (2011).

[146] A. Rusanov, R. Boogaard, M. Hesselberth, H. Sellier, and J. Aarts, Physica C (Amsterdam) **369**, 300 (2002).

[147] A. Rusanov, Ph.D. thesis, University of Leiden, 1977.

[148] D. A. Resnick, K. Gilmore, Y. U. Idzerda, M. T. Klem, M. Allen, T. Douglas, E. Arenholz, and M. Young, J. Appl. Phys. **99**, 08Q501 (2006).

[149] L. He, C. Chen, N. Wang, W. Zhou, and L. Guo, J. Appl. Phys. **102**, 103911 (2007).

[150] P. Dutta, M. S. Seehra, S. Thota, and J. Kumar, J. Phys.: Condens. Matter **20**, 015218 (2008).

[151] Y. A. Kumzerov, N. F. Kartenko, L. S. Parfen'eva, I. A. Smirnov, A. A. Sysoeva, H. Misiorek, and A. Jezowski, Phys. Solid State **54**, 1066 (2012).

[152] W. L. Roth, J. Phys. Chem. Solids **25**, 1 (1963).

[153] G. Blasse, Phillips Res. Rep. **18**, 383 (1963).

[154] C. A. F. Vaz, E. I. Altman, and V. E. Henrich, Phys. Rev. B **81**, 104428 (2010).

[155] W. P. Davey, Phys. Rev. **25**, 753 (1925).

[156] N. W. Ashcroft and N. D. Mermin, *Solid State Physics* (Holt-Saunders, Tokyo, 1981).

[157] J. Crangle, Philos. Mag. **46**, 499 (1955).

[158] J. E. de Miguel, A. Cebollada, J. M. Gallego, S. Ferrer, and R. Miranda, Surf. Sci. **211–212**, 732 (1989).

[159] P. Bruno, Mater. Res. Soc. Symp. Proc. **231**, 299 (1992).

[160] P. Bruno, J. Magn. Soc. Jpn. **15**, 15 (1991).